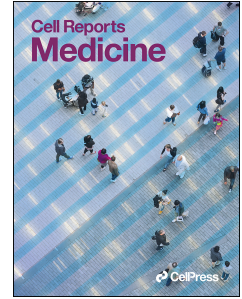


Journal Pre-proof



Cross-reactive coronavirus antibodies with diverse epitope specificities and Fc effector functions

Andrea R. Shiakolas, Kevin J. Kramer, Daniel Wrapp, Simone I. Richardson, Alexandra Schäfer, Steven Wall, Nianshuang Wang, Katarzyna Janowska, Kelsey A. Pilewski, Rohit Venkat, Robert Parks, Nelia P. Manamela, Nagarajan Raju, Emilee Friedman Fechter, Clinton M. Holt, Naveenchandra Suryadevara, Rita E. Chen, David R. Martinez, Rachel S. Nargi, Rachel E. Sutton, Julie E. Ledgerwood, Barney S. Graham, Michael S. Diamond, Barton F. Haynes, Priyamvada Acharya, Robert H. Carnahan, James E. Crowe, Jr., Ralph S. Baric, Lynn Morris, Jason S. McLellan, Ivelin S. Georgiev

PII: S2666-3791(21)00156-7

DOI: <https://doi.org/10.1016/j.xcrm.2021.100313>

Reference: XCRM 100313

To appear in: *Cell Reports Medicine*

Received Date: 22 December 2020

Revised Date: 17 March 2021

Accepted Date: 18 May 2021

Please cite this article as: Shiakolas, A.R., Kramer, K.J., Wrapp, D., Richardson, S.I., Schäfer, A., Wall, S., Wang, N., Janowska, K., Pilewski, K.A., Venkat, R., Parks, R., Manamela, N.P., Raju, N., Fechter, E.F., Holt, C.M., Suryadevara, N., Chen, R.E., Martinez, D.R., Nargi, R.S., Sutton, R.E., Ledgerwood, J.E., Graham, B.S., Diamond, M.S., Haynes, B.F., Acharya, P., Carnahan, R.H., Crowe Jr., J.E., Baric, R.S., Morris, L., McLellan, J.S., Georgiev, I.S., Cross-reactive coronavirus antibodies with diverse epitope specificities and Fc effector functions, *Cell Reports Medicine* (2021), doi: <https://doi.org/10.1016/j.xcrm.2021.100313>.

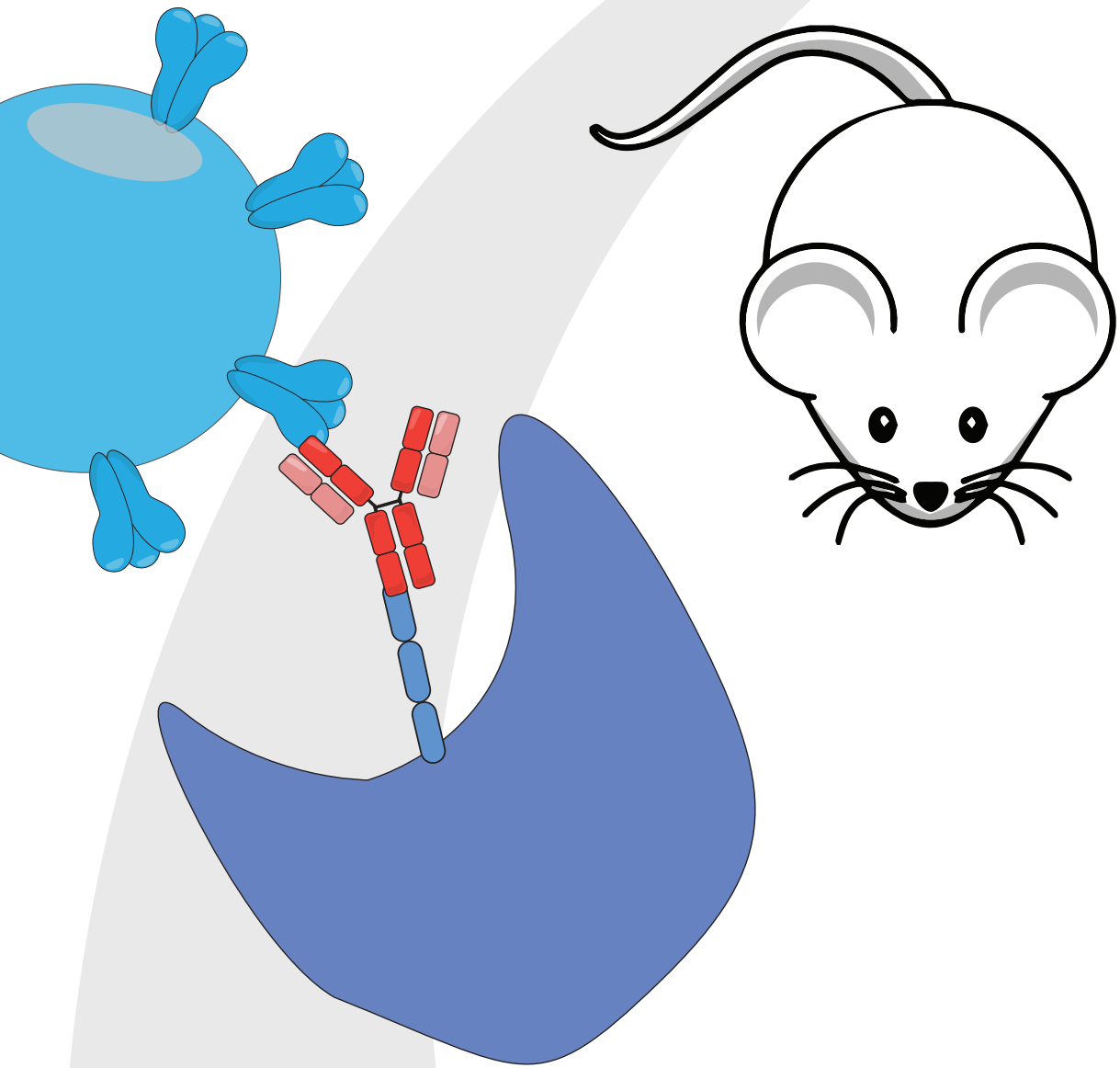
This is a PDF file of an article that has undergone enhancements after acceptance, such as the addition of a cover page and metadata, and formatting for readability, but it is not yet the definitive version of record. This version will undergo additional copyediting, typesetting and review before it is published in its final form, but we are providing this version to give early visibility of the article. Please note that,

during the production process, errors may be discovered which could affect the content, and all legal disclaimers that apply to the journal pertain.

© 2021 The Author(s).

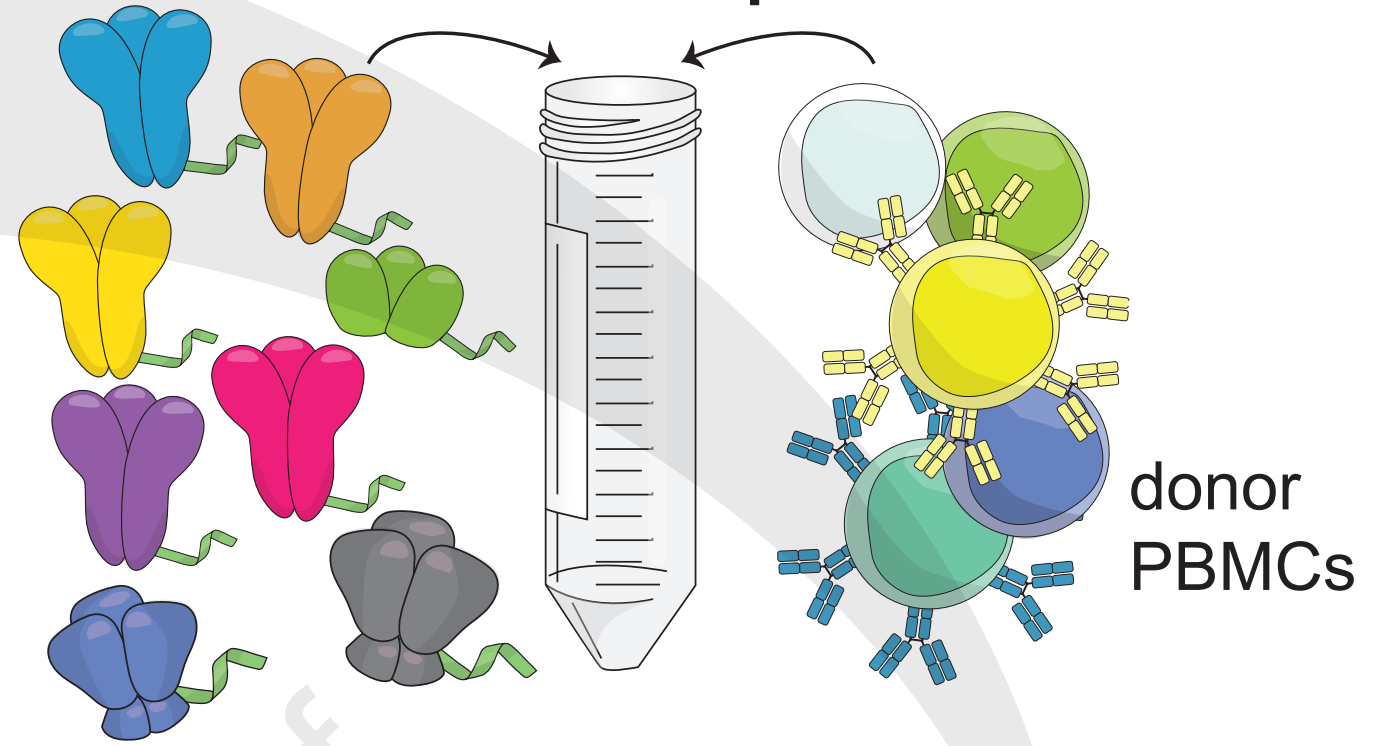
Functional Evaluation and

in vivo Prophylaxis Experiment

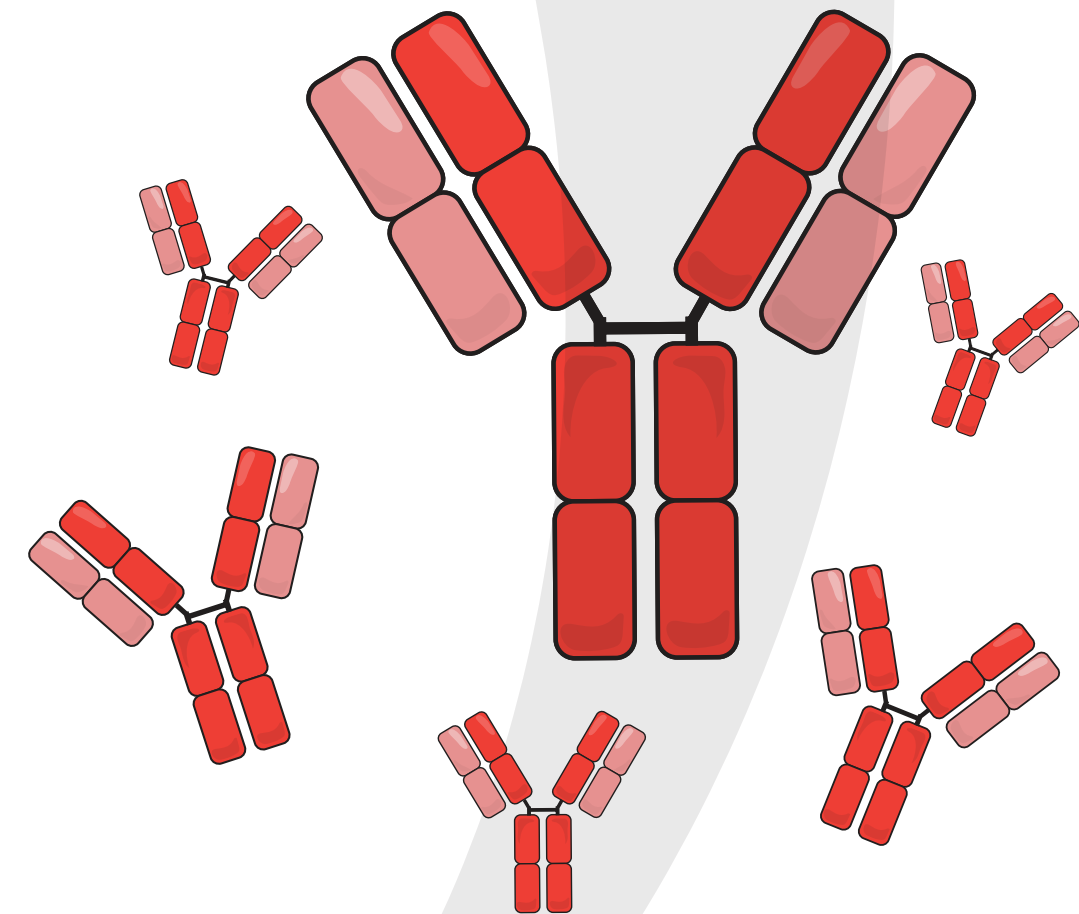


SARS2 S
SARS S
MERS S
MERS S1
OC43 S
HKU1 S
ZM197
CZA97

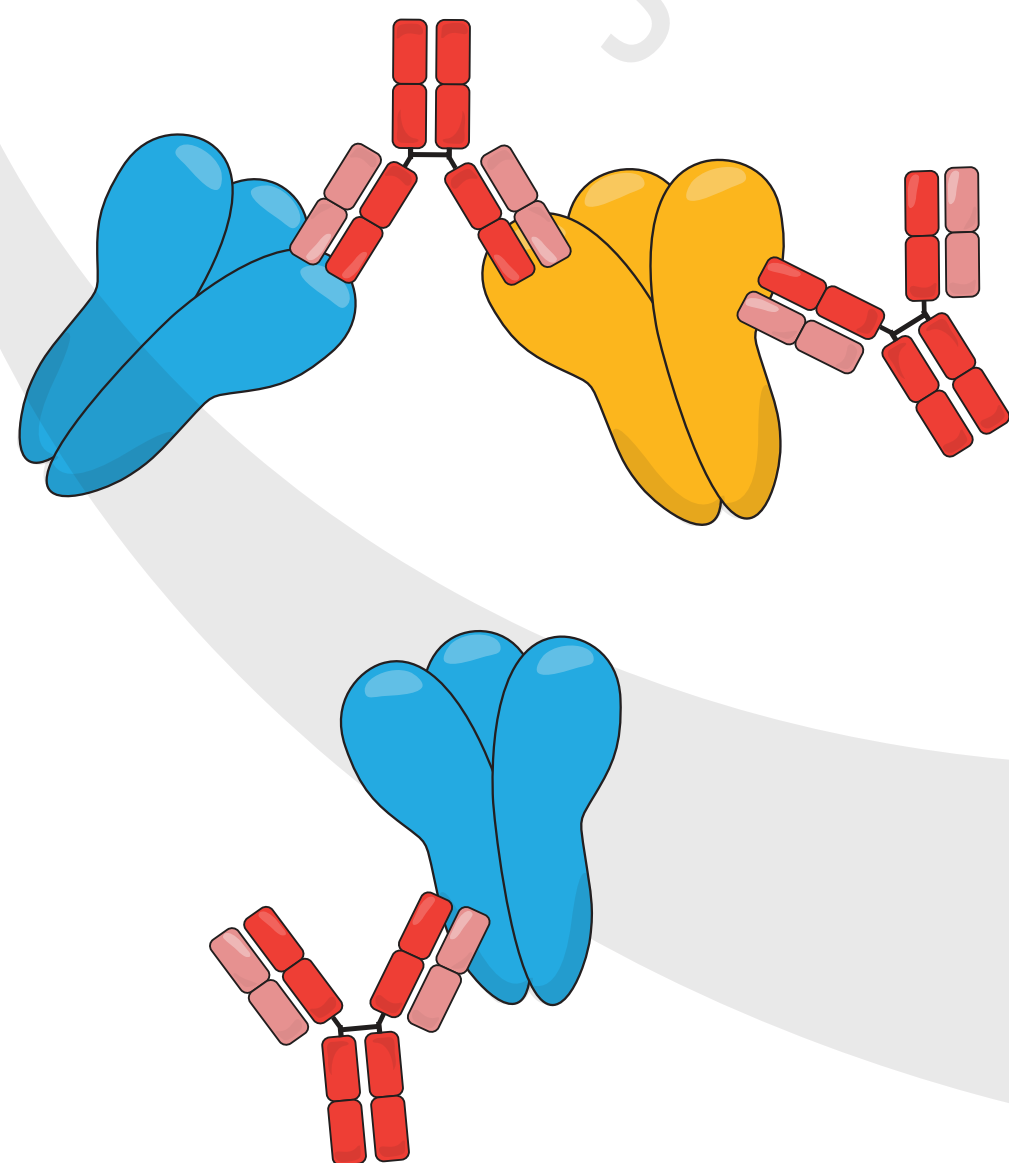
LIBRA-seq



CoV Cross-reactive Antibody Identification



Epitope Mapping



1 **Cross-reactive coronavirus antibodies with diverse epitope specificities and Fc effector**
2 **functions**

3 Andrea R. Shiakolas^{1,2,18}, Kevin J. Kramer^{1,2,18}, Daniel Wrapp³, Simone I. Richardson⁴,
4 Alexandra Schäfer⁵, Steven Wall¹, Nianshuang Wang³, Katarzyna Janowska⁶, Kelsey A.
5 Pilewski^{1,2}, Rohit Venkat^{1,7}, Robert Parks⁸, Nelia P. Manamela⁴, Nagarajan Raju^{1,2}, Emilee
6 Friedman Fechter¹, Clinton M. Holt^{1,7}, Naveenchandra Suryadevara¹, Rita E. Chen^{9,10}, David R.
7 Martinez⁵, Rachel S. Nargi¹, Rachel E. Sutton¹, Julie E. Ledgerwood¹¹, Barney S. Graham¹¹,
8 Michael S. Diamond^{9,10,12}, Barton F. Haynes⁸, Priyamvada Acharya^{6,8}, Robert H. Carnahan^{1,13},
9 James E. Crowe Jr^{1,13}, Ralph S. Baric⁵, Lynn Morris⁴, Jason S. McLellan³, Ivelin S.
10 Georgiev^{1,2,14,15,16,17,19,*}

11
12 ¹Vanderbilt Vaccine Center, Vanderbilt University Medical Center, Nashville, TN, 37232, USA
13 ²Department of Pathology, Microbiology, and Immunology, Vanderbilt University Medical Center,
14 Nashville, TN, 37232, USA
15 ³Department of Molecular Biosciences, The University of Texas at Austin, Austin, TX, 78712,
16 USA
17 ⁴National Institute for Communicable Diseases of the National Health Laboratory Service,
18 Johannesburg 2131, South Africa; Antibody Immunity Research Unit, Faculty of Health
19 Sciences, University of the Witwatersrand, Johannesburg 2193, South Africa.
20 ⁵Department of Epidemiology, University of North Carolina at Chapel Hill, Chapel Hill, NC,
21 27516, USA
22 ⁶Division of Structural Biology, Duke University School of Medicine, Durham, NC, 27710, USA
23 ⁷Program in Chemical and Physical Biology, Vanderbilt University Medical Center, Nashville,
24 TN, 37232, USA
25 ⁸Duke Human Vaccine Institute, Duke University School of Medicine, Durham, NC, 27710, USA

26 ⁹Department of Pathology & Immunology, Washington University School of Medicine, St. Louis,
27 MO, 63110, USA

28 ¹⁰Department of Medicine, Washington University School of Medicine, St. Louis, MO, 63110,
29 USA

30 ¹¹Vaccine Research Center, National Institute of Allergy and Infectious Diseases, National
31 Institutes of Health, Bethesda, MD, 20892, USA

32 ¹²Department of Molecular Microbiology, Washington University School of Medicine, St. Louis,
33 MO, 63110, USA

34 ¹³Department of Pediatrics, Vanderbilt University Medical Center, Nashville, TN, 37232, USA

35 ¹⁴Vanderbilt Institute for Infection, Immunology, and Inflammation, Vanderbilt University Medical
36 Center, Nashville, TN, 37232, USA

37 ¹⁵Department of Electrical Engineering and Computer Science, Vanderbilt University Medical
38 Center, Nashville, TN, 37232, USA

39 ¹⁶Center for Structural Biology, Vanderbilt University, Nashville, TN, 37232, USA

40 ¹⁷Program in Computational Microbiology and Immunology, Vanderbilt University Medical
41 Center, Nashville, TN, 37232, USA

42 ¹⁸These authors contributed equally

43 ¹⁹Lead Contact

44 *Corresponding author: ivelin.georgiev@vanderbilt.edu

45

46

47

48

49 **SUMMARY**

50 The continual emergence of novel coronavirus (CoV) strains, like SARS-CoV-2, highlights the
51 critical need for broadly reactive therapeutics and vaccines against this family of viruses. From a
52 recovered SARS-CoV donor sample, we identify and characterize a panel of six monoclonal
53 antibodies that cross-react with CoV spike (S) proteins from the highly pathogenic SARS-CoV
54 and SARS-CoV-2, and demonstrate a spectrum of reactivity against other CoV. Epitope
55 mapping reveals that these antibodies recognize multiple epitopes on SARS-CoV-2 S, including
56 the receptor binding domain, N-terminal domain, and S2 subunit. Functional characterization
57 demonstrates that the antibodies mediate phagocytosis - and in some cases trogocytosis - but
58 not neutralization *in vitro*. When tested *in vivo* in murine models, two of the antibodies
59 demonstrate a reduction in hemorrhagic pathology in the lungs. The identification of cross-
60 reactive epitopes recognized by functional antibodies expands the repertoire of targets for pan-
61 coronavirus vaccine design strategies.

62

63 INTRODUCTION

64 The emergence of a novel coronavirus (CoV) SARS-CoV-2, the causative agent of COVID-19,
65 has resulted in a worldwide pandemic, threatening the lives of billions and imposing an
66 immense burden on healthcare systems and the global economy. SARS-CoV-2, the seventh
67 coronavirus known to infect humans, is a member of the *Betacoronavirus* genus which includes
68 the highly pathogenic SARS-CoV and MERS-CoV, as well as endemic variants HCoV-OC43
69 and HCoV-HKU1¹. Recent coronavirus outbreaks and the threat of future emerging zoonotic
70 strains highlight the need for broadly applicable coronavirus therapeutic interventions and
71 vaccine design approaches².

72 Coronaviruses utilize the homotrimeric Spike (S) protein to engage with cell-surface receptors
73 and enter host cells. S consists of two functional subunits: S1 and S2. S1 facilitates attachment
74 to target cells and is composed of the N-terminal domain (NTD) and the receptor-binding
75 domain (RBD), whereas S2, which encodes the fusion peptide and heptad repeats, promotes
76 viral fusion^{3,4}. To facilitate cell entry, human coronaviruses employ different host factors;
77 however, SARS-CoV and SARS-CoV-2 both utilize the cell-surface receptor angiotensin
78 converting enzyme 2 (ACE2)⁵. Additionally, SARS-CoV-2 S shares 76% amino acid identity with
79 SARS-CoV S¹. Furthermore, S serves as a dominant antibody target and is a focus of
80 countermeasure development for the treatment and prevention of COVID-19 infection^{6,7}. S
81 proteins from the *Betacoronavirus* genus share multiple regions of structural homology and thus
82 could serve as targets for a cross-reactive antibody response⁸. Identifying cross-reactive
83 antibody epitopes can inform rational design strategies for vaccines and therapies that target
84 multiple highly pathogenic coronaviruses.

85 Numerous potent neutralizing antibodies against SARS-CoV-2 have been discovered, including
86 multiple candidates currently in clinical trials or approved for emergency use for prophylactic

87 and acute treatment of COVID-19⁹⁻¹⁶. Investigation of SARS-CoV-2/SARS-CoV cross-reactive
88 antibodies has focused primarily on the RBD epitope, which has resulted in the identification of
89 a number of SARS-CoV-2/SARS-CoV cross-reactive antibody candidates^{12,17,18}. However, the
90 diversity of epitopes and functions beyond virus neutralization have not been extensively
91 explored for cross-reactive antibodies¹⁹⁻²¹. Evidence of Fc effector function contributing to
92 protection *in vivo* against SARS-CoV²² and SARS-CoV-2²³ suggests that the role of antibodies
93 beyond neutralization may be a crucial component of protection and an important consideration
94 in vaccine design strategies for coronaviruses^{20,24-26}.

95 In this study, we investigated antibody cross-reactivity across the *Betacoronavirus* genus at
96 monoclonal resolution. To do this, we applied LIBRA-seq (Linking B Cell receptor to antigen
97 specificity through sequencing²⁷ to a recovered SARS-CoV donor sample from more than ten
98 years after infection. We identified and characterized SARS-CoV-2/SARS-CoV cross-reactive
99 human antibodies that target multiple, distinct structural domains of S, mediate phagocytosis
100 and trogocytosis, and mitigate pathological burden *in vivo*. A better understanding of the genetic
101 features, epitope specificities, and functional characteristics of cross-reactive coronavirus
102 antibodies may translate into strategies for current vaccine design efforts and additional
103 measures to counteract potential future pandemic strains.

104 **RESULTS**

105 **LIBRA-seq Characterization of a SARS-CoV Recovered Donor**

106 To identify cross-reactive antibodies to multiple coronavirus antigens, LIBRA-seq was applied to
107 a PBMC sample from a donor infected with SARS-CoV over ten years prior to sample collection.
108 The antigen screening library consisted of eight oligo-tagged recombinant soluble antigens: six
109 coronavirus trimer antigens (SARS-CoV-2 S, SARS-CoV S, MERS-CoV S, MERS-CoV S1 (with
110 foldon domain), HCoV-OC43 S, HCoV-HKU1 S) and two HIV trimer antigens from strains

111 ZM197 and CZA97 as negative controls (**Figure 1A**). After the antigen screening library was
112 mixed with donor PBMCs, antigen positive B cells were enriched by fluorescence activated cell
113 sorting and processed for single-cell sequencing (**Supplemental Figure 1A**). After bioinformatic
114 processing, we recovered 2625 cells with paired heavy/light chain sequences and antigen
115 reactivity information (**Supplemental Figure 1B**), and from these cells, there were 2368 unique
116 VDJ sequences. Overall, LIBRA-seq enabled rapid screening of PBMCs from a patient sample,
117 with recovery of paired heavy/light chain sequences and antigen reactivity for thousands of B
118 cells at the single-cell level.

119 **Identification of SARS-CoV-2 and SARS-CoV Cross-reactive Antibodies**

120 With a goal of identifying antibodies that were cross-reactive to multiple coronavirus S proteins,
121 we prioritized lead candidates based on their sequence features and LIBRA-seq scores
122 (**Supplemental Figure 1C**). We selected 15 antibody candidates that exhibited diverse
123 sequence features and utilized a number of different variable genes for expression and
124 characterization (**Figure 1B, Supplemental Figure 1D**). These antibodies displayed a broad
125 range of percent identity to germline (83-98%) and a variety of CDRH3 and CDRL3 lengths (6-
126 24 and 5-13 amino acids, respectively) (**Supplemental Figure 1D**). By ELISA, SARS-CoV-2 S
127 and SARS-CoV S binding was confirmed for 6/15 of the tested antibodies (46472-1, 46472-2,
128 46472-3, 46472-4, 46472-6, and 46472-12), indicating LIBRA-seq could successfully identify
129 SARS-CoV-2 reactive B cells, but also suggesting potential differences in antigen binding
130 detection for primary B cells with a sequencing readout vs. recombinant IgG by ELISA (**Figure**
131 **1C-D, Supplemental Figure 1E**). Further, antibodies 46472-6 and 46472-12 bound to S
132 proteins from endemic HCoV-OC43 and HCoV-HKU1, albeit generally at lower levels (**Figure**
133 **1C-D, Supplemental Figure 1E**). Although the six monoclonal antibodies showed reactivity by
134 ELISA to the MERS-CoV antigen probe used in the LIBRA-seq screening library, antibody
135 binding to other independent preparations of this protein was inconsistent, so MERS-CoV S
136 reactivity could not be confirmed definitively (**Supplemental Figure 1F-G**). Overall, the

137 application of the LIBRA-seq technology enabled the identification of a panel of cross-reactive
138 antibodies that recognize the S antigen from multiple coronaviruses.

139 **Cross-reactive Coronavirus Antibodies Target Diverse Epitopes on S**

140 To elucidate the epitopes targeted by the cross-reactive antibodies, we performed binding
141 assays to various structural domains of S as well as binding-competition experiments. First, we
142 assessed antibody binding to the S1 and S2 subdomains of SARS-CoV-2. Antibodies 46472-1,
143 46472-2, 46472-3, and 46472-4 bound to the S2 domain, whereas 46472-6 and 46472-12
144 recognized the S1 domain but targeted different epitopes, the NTD and RBD, respectively
145 (**Figure 2A-C, Supplemental Figure 2A-B**). Although 46472-12 bound to the RBD, it did not
146 compete with ACE2 for binding to SARS-CoV-2 S and showed partial competition with RBD-
147 directed antibody CR3022 (**Supplemental Figure 2C-D**). To determine whether the antibodies
148 targeted overlapping or distinct epitopes, we performed competition ELISA experiments and
149 found that the S2-directed antibodies 46472-1, 46472-2, and 46472-4 competed for binding to S
150 (**Figure 2D**). This pattern was observed for both SARS-CoV-2 and SARS-CoV S. Of note, this
151 competition group did not include S2-directed antibody 46472-3, revealing the identification of
152 multiple cross-reactive epitope targets on S2 (**Figure 2D**). Further, antibody binding was not
153 affected by two glycan knockout mutants (N165A or N709A) or mannose competition
154 (**Supplemental Figure 2E-F**). Lastly, we measured antibody autoreactivity, and found that with
155 the exception of 46472-6 binding to Jo-1, none of the antibodies showed autoreactivity against
156 the tested antigens (**Figure 2E**). Together, these data suggest that the identified cross-reactive
157 antibodies are coronavirus-specific and target multiple, diverse epitopes on the S protein
158 (**Figure 2F**).

159 **Functional Characterization of Cross-reactive Coronavirus Antibodies**

160 Next, we characterized our cross-reactive antibody panel for functional activity. Although none
161 of the antibodies neutralized SARS-CoV or SARS-CoV-2 (**Supplemental Figure 3A-B**), all
162 antibodies showed antibody-dependent cellular phagocytosis (ADCP) *in vitro* for SARS-CoV-2 S

163 **(Figure 3A)**. In particular, the RBD-reactive antibody 46472-12 showed greater ADCP activity
164 compared to the other cross-reactive antibodies and the SARS-CoV/SARS-CoV-2 cross-
165 reactive RBD antibody control, CR3022²⁸ **(Figure 3A, Supplemental Figure 3C)**. Further, we
166 tested and confirmed ADCP activity against SARS-CoV for two antibodies that mediated the
167 highest phagocytotic activity against SARS-CoV-2, 46472-4 and 46472-12, illustrating that these
168 antibodies have cross-coronavirus phagocytic ability **(Figure 3B, Supplemental Figure 3D)**.
169 We next tested the antibodies in a trogocytosis assay²⁹ and found that four antibodies in our
170 panel (46472-1, 46472-2, 46472-3, and 46472-4) mediated trogocytosis **(Figure 3C,**
171 **Supplemental Figure 3E)**. This warrants further investigation as this is the first description of
172 trogocytosis performed by SARS-CoV-2 specific mAbs. Lastly, none of the antibodies promoted
173 complement deposition (ADCD) **(Figure 3D, Supplemental Figure 3F)**. Together, these results
174 revealed different profiles of Fc effector functionality within the panel of cross-reactive
175 antibodies.

176 Since non-neutralizing SARS-CoV-2 antibodies with Fc effector function activity have not been
177 extensively characterized *in vivo*, these results prompted us to test antibodies 46472-4 and
178 46472-12 for prophylaxis in a murine infection model using a mouse-adapted virus strain
179 (SARS-CoV-2 MA)^{30,31} at a non-lethal dose of 1×10^3 PFU **(Figure 4A)**. Although there were no
180 differences in survival and viral load between experimental and control groups, the lung
181 hemorrhage scores (see Methods) for 46472-4 and 46472-12 were similar to antigen-specific
182 control CR3022, and all three groups were significantly lower than the scores for isotype control
183 DENV-2D22 ($p < 0.01$, ordinary one-way ANOVA with multiple comparisons) **(Figure 4B,**
184 **Supplemental Figure 4A)**. To evaluate the *in vivo* effect of these antibodies in a more stringent
185 challenge model in 12-month old female BALB/c mice, we increased the viral dose from 1×10^3
186 to 1×10^4 PFU. In this experiment, mice that received antibody 46472-12 exhibited the best
187 survival rate (4/5 at day 4), compared to the other treatment groups that included CR3022 as an
188 antigen-specific control and DENV-2D22 as a negative control, although statistical significance

189 was not achieved (**Figure 4C-D, Supplemental Figure 4B**). There were no significant
190 differences in viral load between groups; however, the surviving animals from the 46472-4 and
191 46472-12 groups showed significantly lower hemorrhagic pathology scores in harvested mouse
192 lungs compared to the negative control treatment group ($p < 0.001$, ordinary one-way ANOVA
193 with multiple comparisons) (**Figure 4C**). Animals treated with the antigen-specific control,
194 CR3022, had significantly higher hemorrhage scores than animals treated with 46472-4 and
195 46472-12 ($p < 0.001$, ordinary one-way ANOVA with multiple comparisons), although the
196 statistical analysis may be limited by the small numbers of surviving animals for some of the
197 groups (**Figure 4C**). While definitive evidence for protection is limited, the data from the *in vivo*
198 experiments suggests that these cross-reactive antibodies could contribute to counteracting
199 coronavirus infection in prophylaxis.

200

201 **DISCUSSION**

202 Here, we described a set of cross-reactive *Betacoronavirus* antibodies isolated from a
203 recovered SARS-CoV donor. The antibodies targeted diverse epitopes on S, including the S2
204 subdomain as well as the RBD and NTD on S1, and demonstrated Fc effector function *in vitro*.
205 Additionally, two of these antibodies were tested *in vivo*, and displayed a reduction in lung
206 hemorrhage score, while effects on viral load were not definitive.

207 Given the similar effect of 46472-4 and 46472-12 on severe disease in the mouse model, their
208 phagocytotic ability along with the inability to mediate neutralization suggests that the former
209 may be a mechanism through which they function, and additional studies are underway to
210 further assess this hypothesis. Phagocytosis has been shown to be associated with protection
211 in a SARS-CoV-2 DNA vaccination in non-human primates as well as survival in natural
212 infection³³ and as such could be an important mechanism for protection by monoclonal
213 antibodies. The role of trogocytosis in COVID-19 is unknown as are the targets that may be

214 important for this function. 46472-4 was able to mediate this membrane nibbling in contrast to
215 46472-12, suggesting that this function in addition to complement activity was not responsible
216 for the *in vivo* effect on severe disease mediated by these antibodies. Although the precise *in*
217 *vivo* effects of these antibodies have not been elucidated, the identification of multiple, cross-
218 reactive antibodies highlights a potential role for Fc effector function activity, specifically
219 phagocytosis, in coronavirus infection. Evidence of protection associated with Fc effector
220 function in SARS-CoV²², SARS-CoV-2^{23,24,34}, and other infectious diseases including influenza,
221 Ebola, and HIV, motivates further investigation into its contribution for the treatment of COVID-
222 19³⁵⁻³⁸. Furthermore, the importance of Fc effector functionality of potentially neutralizing
223 candidate clinical SARS-CoV-2 mAbs in a therapeutic setting rather than prophylaxis highlights
224 the potential benefit for investigation into non-neutralizing antibodies with phagocytic activity and
225 their administration after infection onset³⁹. Elucidation of the functional roles of cross-reactive
226 but non-neutralizing antibodies could have implications for understanding the factors involved in
227 protection or enhancement of disease.

228 Given the ongoing SARS-CoV-2 pandemic and the potential for future zoonotic coronavirus
229 pathogens to emerge, coronavirus vaccine and therapeutic development is of paramount
230 importance⁴⁰⁻⁴³. Antibodies that can cross-react with multiple coronavirus strains are primary
231 targets as potential broadly reactive therapies. Such antibodies can further reveal cross-reactive
232 epitopes that could serve as templates for the development of broadly protective vaccines.
233 Understanding the spectrum of cross-reactive epitopes targeted by human antibodies, as well
234 as the functional role that such antibodies have within coronavirus infection, are therefore a vital
235 element of medical countermeasure development.

236 **Limitations of the Study**

237 The current study focuses on the characterization of cross-reactive coronavirus antibodies,
238 mostly in the context of SARS-CoV-2. Further characterization of this panel of antibodies

239 against circulating endemic coronavirus strains would enhance the clinical relevance to less
240 severe coronavirus-associated respiratory infections.

241 The current study utilized a dosing regimen in a prophylactic setting and given the emerging
242 evidence of survival benefit with effector function in antibodies given after infection onset³⁹,
243 antibody administration in a therapeutic setting may provide further insight into *in vivo*
244 properties. Furthermore, additional effector function characterization such as ADCC and ADNP
245 would strengthen the profile of this panel of non-neutralizing antibodies given their role in both
246 human⁴⁴ and mouse SARS-CoV-2 infection studies.

247 **ACKNOWLEDGEMENTS**

248 We thank Angela Jones, Latha Raju, and Jamie Roberson of Vanderbilt Technologies for
249 Advanced Genomics for their expertise regarding NGS and library preparation; David Flaherty
250 and Brittany Matlock of the Vanderbilt Flow Cytometry Shared Resource for help with flow panel
251 optimization; and members of the Georgiev laboratory for comments on the manuscript. The
252 Vanderbilt VANTAGE Core provided technical assistance for this work. VANTAGE is supported
253 in part by CTSA grant 5UL1 RR024975-03, the Vanderbilt Ingram Cancer Center (P30
254 CA68485), the Vanderbilt Vision Center (P30 EY08126), and NIH/NCRR (G20 RR030956). This
255 work was conducted in part using the resources of the Advanced Computing Center for
256 Research and Education at Vanderbilt University (Nashville, TN). Flow cytometry experiments
257 were performed in the VUMC Flow Cytometry Shared Resource. The VUMC Flow Cytometry
258 Shared Resource is supported by the Vanderbilt Ingram Cancer Center (P30 CA68485) and the
259 Vanderbilt Digestive Disease Research Center (DK058404).

260 For work described in this manuscript, I.S.G., A.R.S., K.J.K., S.W., K.A.P., R.V., N.R., E.F.F.,
261 C.M.H. were supported in part by NIH NIAID award R01AI131722-S1, the Hays Foundation
262 COVID-19 Research Fund, Fast Grants, and CTSA award No. UL1 TR002243 from the National

263 Center for Advancing Translational Sciences. J.S.M and D.W. were supported in part by a
264 National Institutes of Health (NIH)/National Institute of Allergy and Infectious Diseases (NIAID)
265 grant awarded to J.S.M. (R01-AI127521). L.M. and S.I.R. acknowledge research funding from
266 the South African Medical Research Council (MRC) Extramural Unit and SHIP-COVID19
267 programs and an H3 Africa grant (U01A136677). S.I.R. is supported by the South African
268 Research Chairs Initiative of the Department of Science and Technology and the NRF (Grant
269 No 98341) and is a L'Oreal/UNESCO South Africa Young Talents Awardee. R.B., A.S., D.R.M.,
270 were supported by NIH grants (U54CA260543, R01AI157155). P.A. and K.J. were supported by
271 NIH grant R01 AI14567. J.E.C., R.H.C., N.S., R.N.S., and R.E.S., were supported by Defense
272 Advanced Research Projects Agency (DARPA) grants HR0011-18-2-0001 and HR00 11-18-3-
273 0001; NIH contracts 75N93019C00074 and 75N93019C00062; NIH grants U01 AI150739, R01
274 AI130591 and R35 HL145242; the Dolly Parton COVID-19 Research Fund at Vanderbilt; and
275 NIH grant S10 RR028106 for the Next Generation Nucleic Acid Sequencer, housed in
276 VANTAGE. M.S.D. and R.E.C. were supported by grants from NIH (R01 AI157155) and the
277 Defense Advanced Research Project Agency (HR001117S0019). B.F.H. and R.P. were
278 supported by NC State funding for COVID research. B.S.G. was supported by intramural
279 funding from the NIAID. C.M.H. was supported in part by NIH grant T32 GM008320-30. D.R.M.
280 was supported by an NIH F32 AI152296, a Burroughs Wellcome Fund Postdoctoral Enrichment
281 Program Award, and was previously supported by an NIH NIAID T32 AI007151.

282 **AUTHOR CONTRIBUTIONS**

283 Methodology, A.R.S., K.J.K., and I.S.G.; Investigation, A.R.S., K.J.K., D.W., S.I.R., A.S., S.W.,
284 N.W., K.J., K.A.P., R.V., R.P., N.P.M., N.R., E.F.F., C.M.H., N.S., R.E.C., D.R.M., R.S.N.,
285 R.E.S., J.E.L., B.S.G., M.S.D., B.F.H., P.A., R.H.C., J.E.C., R.S.B., L.M., J.S.M., and I.S.G.;
286 Software, A.R.S., R.V., N.R.; Validation, A.R.S., K.J.K.; Writing - Original Draft, A.R.S., and
287 K.J.K.; Writing -Review & Editing, all authors; Funding Acquisition, I.S.G., B.S.G., M.S.D.,

288 B.F.H., P.A., R.H.C., J.E.C., R.S.B., L.M., J.S.M., and A.R.S, and K.J.K.; Resources, B.S.G.,
289 M.S.D., B.F.H., P.A., R.H.C., J.E.C., R.S.B., L.M., J.S.M., and I.S.G.; Supervision, I.S.G.

290

291 **DECLARATION OF INTERESTS**

292 A.R.S. and I.S.G are co-founders of AbSeek Bio. A.R.S., K.J.K, I.S.G., D.W., N.W., and J.S.M
293 are listed as inventors on patents filed describing the antibodies described here. D.W., J.S.M,
294 B.S.G, and N.W. are also listed as inventors on U.S. patent application no. 62/972,886 (2019-
295 nCoV Vaccine). M.S.D. is a consultant for Inbios, Vir Biotechnology, NGM Biopharmaceuticals,
296 and Carnival Corporation and on the Scientific Advisory Boards of Moderna and Immunome.
297 The Diamond laboratory has unrelated sponsored research agreements from Emergent
298 BioSolutions, Moderna and Vir Biotechnology. J.E.C. has served as a consultant for Eli Lilly,
299 GlaxoSmithKline and Luna Biologics, is a member of the Scientific Advisory Boards of
300 CompuVax and Meissa Vaccines and is Founder of IDBiologics. The Crowe laboratory at
301 Vanderbilt University Medical Center has received sponsored research agreements from
302 IDBiologics and AstraZeneca. R.S.B. has competing interests associated with Eli Lily, Takeda
303 and Pfizer. The Georgiev laboratory at Vanderbilt University Medical Center has received
304 unrelated funding from Takeda Pharmaceuticals.

305 **FIGURE CAPTIONS**

306 **Figure 1. Identification of coronavirus cross-reactive antibodies from SARS-CoV**
307 **recovered PBMC sample using LIBRA-seq, see also Figure S1.**

308 (A) Schematic of DNA-barcoded antigens used to probe a SARS-CoV donor PBMC sample.

309 (B) LIBRA-seq scores for SARS-CoV (x-axis) and SARS-CoV-2 (y-axis) for all IgG cells
310 recovered from sequencing are shown as circles. 15 lead antibody candidates are highlighted in
311 purple.

312 (C) Antibodies were tested for binding to CoV antigens by ELISA. HIV-specific antibody VRC01
313 was used as a negative control. Anti-SARS-CoV mouse antibody 240CD was also used.

314 ELISAs were performed in technical duplicates with at least two biological duplicates. Data are
315 represented as mean \pm SEM.

316 (D) ELISA binding data are displayed as a heatmap of the AUC values calculated from data in
317 Figure 1C, with AUC of 0 as white, and maximum AUC as purple.

318 **Figure 2. Epitope mapping of cross-reactive antibodies, see also Figure S2.**

319 (A) For cross-reactive coronavirus antibodies, ELISA data against the antigens are displayed as
320 a heatmap of the AUC values calculated from the data in Figure S2A. (B) For SARS-CoV-2 S1
321 reactive antibodies, ELISA data against the RBD and NTD are displayed as a heatmap of the
322 AUC values calculated from the data in Figure S2B. AUC of 0 is displayed as white and
323 maximum AUC as purple. ELISA data are representative of at least two independent
324 experiments. Anti-HIV antibody VRC01 and anti-VEGF antibody are shown as a negative
325 control, and anti-SARS-CoV antibody 240CD is shown as a positive control.

326 (C) Surface plasmon resonance binding of 46472-12 Fab to SARS-CoV-2 RBD. Affinity
327 measurements are shown to the right of the graph.

328 (D) Cross-reactive antibodies were used in a competition ELISA to determine if binding of one
329 antibody affected binding of another. Competitor antibodies were added at 10 μ g/ml, and then
330 detected antibodies were added at 0.1 μ g/ml. The percent reduction in binding compared to
331 binding without a competitor is shown. An anti-HIV antibody was used as a negative control.
332 ELISAs were performed in technical duplicates with at least two biological duplicates.

333 (E) Antibodies were tested for autoreactivity against a variety of antigens in the Luminex
334 AtheNA assay. AU stands for Athena Units. Anti-HIV antibody 4E10 was used as a positive
335 control and Ab82 was used as a negative control.

336 (F) Cross-reactive coronavirus antibodies target a variety of epitopes on the SARS-CoV-2 S
337 protein, including the RBD, NTD, and S2 domains, highlighted on the structure (PDB: 6VSB).

338 **Figure 3. Functional activity of cross-reactive coronavirus antibodies, see also Figure S3.**

339 (A) Cross-reactive coronavirus antibodies were tested for antibody-dependent cellular
340 phagocytosis activity (ADCP) against SARS-CoV-2 S, compared to positive control CR3022 and
341 negative control Palivizumab, an anti-RSV antibody. AUC of the phagocytosis score is shown,
342 calculated from data in Figure S3C. Data are represented as mean \pm SD.

343 (B) 46472-4 and 46472-12 were tested for ADCP activity against SARS-CoV S, compared to
344 CR3022 and anti-RSV Palivizumab. AUC of the phagocytosis score is shown, calculated from
345 data in Figure S3D. Data are represented as mean \pm SD.

346 (C) Cross-reactive coronavirus antibodies were tested for antibody-dependent cellular
347 trogocytosis (ADCT) activity against SARS-CoV-2 S displayed on transfected cells, compared to
348 positive control CR3022 and anti-RSV Palivizumab. AUC of the trogocytosis score is shown,
349 calculated from data in Figure S3E. Data are represented as mean \pm SD.

350 (D) Cross-reactive coronavirus antibodies were tested for antibody-dependent complement
351 deposition (ADCD) activity against SARS-CoV-2 S, compared to positive control CR3022 and
352 anti-RSV Palivizumab. AUC of the C3b deposition score is shown, calculated from data in
353 Figure S3F. Data are represented as mean \pm SD.

354 **Figure 4. *In vivo* effects of cross-reactive antibodies, see also Figure S4.**

355 (A) Timeline of the prophylactic antibody experiment in SARS-CoV-2 mouse adapted (MA) *in*
356 *vivo* infection model.

357 (B,C) For each antibody treatment group for the experiment utilizing (B) 1×10^3 PFU or (C) 1×10^4
358 PFU of SARS-CoV-2 MA, shown are daily body weight progression, and terminal RT-qPCR
359 quantification of lung viral titer and lung hemorrhage scores of gross pathology. For viral titer
360 values and the lung hemorrhage scores, an ordinary one-way ANOVA test with multiple
361 comparisons was performed.

362 (D) For the experiment with 1×10^4 PFU of SARS-CoV-2 MA, percent survival for each antibody
363 group is shown.

364

365 STAR Methods**366 RESOURCE AVAILABILITY****367 Lead Contact**

368 Further information and requests for resources and reagents should be directed to the Lead
369 Contact, Ivelin Georgiev (Ivelin.Georgiev@Vanderbilt.edu).

370 Materials Availability

371 All unique/stable reagents generated in this study are available from the Lead Contact with a
372 completed Materials Transfer Agreement. Please direct resource and reagent requests to the
373 Lead Contact specified above, Ivelin Georgiev.

374 Data and Code Availability

375 Sequences for antibodies identified and characterized in this study have been deposited to
376 GenBank under GenBank accession numbers MZ126644-MZ126658 (heavy chain) and
377 MZ126659-MZ126673 (light chain). Raw sequencing data used in this study are available on the
378 Sequence Read Archive under BioProject accession number PRJNA727275. Custom scripts
379 used to analyze data in this manuscript are available upon request to the corresponding author.

380

381 EXPERIMENTAL MODEL AND SUBJECT DETAILS**382 Human subjects**

383 The donor had prior SARS-CoV infection during the 2004 outbreak in Hong Kong, and the
384 PBMC sample was collected over 10 years post infection (20 million PBMCs). Additional
385 information about the donor is not available.

386

387 Cell lines

388 A variety of cell lines were utilized for various assays in this study.

389 Expi293F mammalian cells (ThermoFisher) were maintained in FreeStyle F17 expression
390 medium supplemented at final concentrations of 0.1% Pluronic Acid F-68 and 20% 4mM L-
391 Glutamine. These cells were cultured at 37°C with 8% CO₂ saturation and shaking.
392 FreeStyle293F cells were grown while shaking at 37 C in 8% CO₂ and 80% humidity.
393 Freestyle293F cells are derived from female human embryonic kidney epithelial cells.
394 THP-1 cells obtained from the AIDS Reagent Program (Division of AIDS, NIAID, NIH
395 contributed by Dr. Li Wu and Vineet N. KewalRamani) were used for both the ADCP and ADCT
396 assays. Cells were cultured at 37°C, 5% CO₂ in RPMI containing 10% heat-inactivated fetal
397 bovine serum (Gibco, Gaithersburg, MD), 1% Penicillin Streptomycin (Gibco, Gaithersburg, MD)
398 and 2-mercaptoethanol to a final concentration of 0.05 mM. These cells were not allowed to
399 exceed 4 x 10⁵ cells/ml to prevent differentiation and are from a male donor.
400 HEK293T cells were obtained from Dr George Shaw and were used for the ADCT assay. These
401 adherent cell lines were cultured at 37°C, 5% CO₂, in DMEM containing 10% heat-inactivated
402 fetal bovine serum (Gibco BRL Life Technologies) and supplemented with 50 µg/ml gentamicin
403 (Sigma). Cells were disrupted at confluence with 0.25% trypsin in 1 mM EDTA (Sigma) every
404 48–72 hours. HEK293F suspension cells were cultured in 293Freestyle media (Gibco BRL Life
405 Technologies) and grown in a shaking incubator at 37°C, 5% CO₂, 70% humidity at 125rpm.
406 Cells were diluted twice a week to between 0.2 and 0.5 million cells/ml. Both HEK293 derived
407 cell lines are from female donors.

408

409 **Murine Model**

410 12-month old female BALB/c mice (BALB/cAnHsd; Envigo, stock number 047) were used in a
411 murine infection model for SARS-CoV-2 with a mouse adapted strain.

412 Eleven to twelve-month old female BALB/c mice (BALB/c AnNHsd, Envigo, stock# 047) were
413 used for mouse-adapted SARS-CoV-2 (SARS-CoV-2 MA10) *in vivo* protection experiments as
414 described previously³¹. All mouse studies were performed at the University of North Carolina

415 (Animal Welfare Assurance #A3410-01) using protocols (19-168) approved by the UNC
416 Institutional Animal Care and Use Committee (IACUC) and were performed in a BSL3 facility at
417 UNC.

418

419 **METHOD DETAILS**

420 **Antigen Purification**

421 A variety of recombinant soluble protein antigens were used in the LIBRA-seq experiment and
422 other experimental assays.

423

424 Plasmids encoding residues 1–1208 of the SARS-CoV-2 spike with a mutated S1/S2 cleavage
425 site, proline substitutions at positions 986 and 987, and a C-terminal T4-fibrin trimerization
426 motif, an 8x HisTag, and a TwinStrepTag (SARS-CoV-2 S-2P); residues 1-1190 of the SARS-
427 CoV spike with proline substitutions at positions 968 and 969, and a C-terminal T4-fibrin
428 trimerization motif, an 8x HisTag, and a TwinStrepTag (SARS-CoV S-2P); residues 1-1291 of
429 the MERS-CoV spike with a mutated S1/S2 cleavage site, proline substitutions at positions
430 1060 and 1061, and a C-terminal T4-fibrin trimerization motif, an AviTag, an 8x HisTag, and a
431 TwinStrepTag (MERS-CoV S-2P Avi); residues 1-751 of the MERS-CoV spike with a C-terminal
432 T4-fibrin trimerization motif, 8x HisTag, and a TwinStrepTag (MERS-CoV S1); residues 1-1277
433 of the HCoV-HKU1 spike with a mutated S1/S2 cleavage site, proline substitutions at positions
434 1067 and 1068, and a C-terminal T4-fibrin trimerization motif, an 8x HisTag, and a
435 TwinStrepTag (HCoV-HKU1 S-2P); residues 1-1278 of the HCoV-OC43 spike with proline
436 substitutions at positions 1070 and 1071, and a C-terminal T4-fibrin trimerization motif, an 8x
437 HisTag, and a TwinStrepTag (HCoV-OC43 S-2P); or residues 319–591 of SARS-CoV-2 S with
438 a C-terminal monomeric human IgG Fc-tag and an 8x HisTag (SARS-CoV-2 RBD-SD1) were
439 transiently transfected into FreeStyle293F cells (Thermo Fisher) using polyethylenimine. The
440 coronavirus trimer spike antigens were in a prefusion-stabilized (S-2P) conformation that better

441 represents neutralization-sensitive epitopes in comparison to their wild-type forms⁴⁵. Two hours
442 post-transfection, cells were treated with kifunensine to ensure uniform glycosylation.
443 Transfected supernatants were harvested after 6 days of expression. SARS-CoV-2 RBD-SD1
444 was purified using Protein A resin (Pierce), SARS-CoV-2 S-2P, SARS-CoV S-2P, MERS-CoV
445 S-2P Avi, MERS-CoV S1, HCoV-HKU1 S-2P and HCoV-OC43 S-2P were purified using
446 StrepTactin resin (IBA). Affinity-purified SARS-CoV-2 RBD-SD1 was further purified over a
447 Superdex75 column (GE Life Sciences). MERS-CoV S1 was purified over a Superdex200
448 Increase column (GE Life Sciences). SARS-CoV-2 S-2P, SARS-CoV S-2P, MERS-CoV S-2P
449 Avi, HCoV-HKU1 S-2P and HCoV-OC43 S-2P were purified over a Superose6 Increase column
450 (GE Life Sciences).

451

452 For the HIV-1 gp140 SOSIP variant from strain ZM197 (clade C) and CZA97 (clade C),
453 recombinant, soluble antigens contained an AviTag and were expressed in Expi293F cells using
454 polyethylenimine transfection reagent and cultured. FreeStyle F17 expression medium
455 supplemented with pluronic acid and glutamine was used. The cells were cultured at 37°C with
456 8% CO₂ saturation and shaking. After 5-7 days, cultures were centrifuged and supernatant was
457 filtered and run over an affinity column of agarose bound *Galanthus nivalis* lectin. The column
458 was washed with PBS and antigens were eluted with 30 mL of 1M methyl- α -D-
459 mannopyranoside. Protein elutions were buffer exchanged into PBS, concentrated, and run on a
460 Superdex 200 Increase 10/300 GL Sizing column on the AKTA FPLC system. Fractions
461 corresponding to correctly folded protein were collected, analyzed by SDS-PAGE and
462 antigenicity was characterized by ELISA using known monoclonal antibodies specific to each
463 antigen. Avi-tagged antigens were biotinylated using BirA biotin ligase (Avidity LLC). Non-Avi-
464 tagged antigens were biotinylated using the EZ-Link Sulfo-NHS-Biotin kits using a 50:1 biotin to
465 protein molar ratio.

466

467 For binding studies, SARS-CoV-2 HexaPro S, SARS-CoV S, SARS-CoV-2 RBD, SARS-CoV
468 RBD, and MERS-CoV RBD constructs were expressed in the transient expression system
469 previously mentioned. S proteins were purified using StrepTrap HP columns and RBD
470 constructs were purified over protein A resin, respectively. Each resulting protein was further
471 purified to homogeneity by size-exclusion chromatography on a Superose 6 10/300 GL column.

472
473 SARS-CoV-2 S1, SARS-CoV-2 S1 D614G, SARS-CoV-2 S2, and SARS-CoV-2 NTD truncated
474 proteins were purchased from the commercial vendor, Sino Biological.

475

476 **DNA-barcoding of Antigens**

477 We used oligos that possess 15 bp antigen barcode, a sequence capable of annealing to the
478 template switch oligo that is part of the 10X bead-delivered oligos, and contain truncated
479 TruSeq small RNA read 1 sequences in the following structure: 5'-
480 CCTTGGCACCCGAGAATTCCANNNNNNNNNNNNNNCCCATATAAGA*A*A-3', where Ns
481 represent the antigen barcode. We used the following antigen barcodes: GTCCTTTACACGTA
482 (SARS-CoV-2 S), TGACCTTCCTCTCCT (SARS-CoV S), ACAATTTGTCTGCGA (MERS-CoV
483 S), TCCTTTCCTGATAGG (MERS-CoV S1), CAGGTCCCTTATTTTC (HCoV-HKU1 S),
484 TAACTCAGGGCCTAT (HCoV-OC43 S), CAGCCCACTGCAATA (CZA97), and
485 ATCGTCGAGAGCTAG (ZM197). Oligos were ordered from IDT with a 5' amino modification
486 and HPLC purified.

487

488 For each antigen, a unique DNA barcode was directly conjugated to the antigen itself. In
489 particular, 5' amino-oligonucleotides were conjugated directly to each antigen using the Solulink
490 Protein-Oligonucleotide Conjugation Kit (TriLink cat no. S-9011) according to manufacturer's
491 instructions. Briefly, the oligo and protein were desalted, and then the amino-oligo was modified
492 with the 4FB crosslinker, and the biotinylated antigen protein was modified with S-HyNic. Then,

493 the 4FB-oligo and the HyNic-antigen were mixed together. This causes a stable bond to form
494 between the protein and the oligonucleotide. The concentration of the antigen-oligo conjugates
495 was determined by a BCA assay, and the HyNic molar substitution ratio of the antigen-oligo
496 conjugates was analyzed using the NanoDrop according to the Solulink protocol guidelines.
497 AKTA FPLC was used to remove excess oligonucleotide from the protein-oligo conjugates,
498 which were also verified using SDS-PAGE with a silver stain. Antigen-oligo conjugates were
499 also used in flow cytometry titration experiments.

500

501 **Antigen specific B cell sorting**

502 Cells were stained and mixed with DNA-barcoded antigens and other antibodies, and then
503 sorted using fluorescence activated cell sorting (FACS). First, cells were counted and viability
504 was assessed using Trypan Blue. Then, cells were washed three times with DPBS
505 supplemented with 0.1% Bovine serum albumin (BSA). Cells were resuspended in DPBS-BSA
506 and stained with cell markers including viability dye (Ghost Red 780), CD14-APC-Cy7, CD3-
507 FITC, CD19-BV711, and IgG-PE-Cy5. Additionally, antigen-oligo conjugates were added to the
508 stain. After staining in the dark for 30 minutes at room temperature, cells were washed three
509 times with DPBS-BSA at 300 g for five minutes. Cells were then incubated for 15 minutes at
510 room temperature with Streptavidin-PE to label cells with bound antigen. Cells were washed
511 three times with DPBS-BSA, resuspended in DPBS, and sorted by FACS. Antigen positive cells
512 were bulk sorted and delivered to the Vanderbilt Technologies for Advanced Genomics
513 (VANTAGE) sequencing core at an appropriate target concentration for 10X Genomics library
514 preparation and subsequent sequencing. FACS data were analyzed using FlowJo.

515

516 **Sample and Library Preparation, and Sequencing**

517 Single-cell suspensions were loaded onto the Chromium Controller microfluidics device (10X
518 Genomics) and processed using the B-cell Single Cell V(D)J solution according to

519 manufacturer's suggestions for a target capture of 10,000 B cells per 1/8 10X cassette, with
520 minor modifications in order to intercept, amplify and purify the antigen barcode libraries as
521 previously described²⁷.

522

523 **Sequence Processing and Bioinformatic Analysis**

524 We utilized and modified our previously described pipeline to use paired-end FASTQ files of
525 oligo libraries as input, process and annotate reads for cell barcode, UMI, and antigen barcode,
526 and generate a cell barcode - antigen barcode UMI count matrix²⁷. BCR contigs were processed
527 using Cell Ranger (10X Genomics) using GRCh38 as reference. Antigen barcode libraries were
528 also processed using Cell Ranger (10X Genomics). The overlapping cell barcodes between the
529 two libraries were used as the basis of the subsequent analysis. We removed cell barcodes that
530 had only non-functional heavy chain sequences as well as cells with multiple functional heavy
531 chain sequences and/or multiple functional light chain sequences, reasoning that these may be
532 multiplets. Additionally, we aligned the BCR contigs (filtered_contigs.fasta file output by Cell
533 Ranger, 10X Genomics) to IMGT reference genes using HighV-Quest⁴⁶. The output of HighV-
534 Quest was parsed using ChangeO⁴⁷ and merged with an antigen barcode UMI count matrix.
535 Finally, we determined the LIBRA-seq score for each antigen in the library for every cell as
536 previously described²⁷.

537

538 **Antibody Expression and Purification**

539 For each antibody, variable genes were inserted into custom plasmids encoding the constant
540 region for the IgG1 heavy chain as well as respective lambda and kappa light chains (pTwist
541 CMV BetaGlobin WPRE Neo vector, Twist Bioscience). Antibodies were expressed in Expi293F
542 mammalian cells (ThermoFisher) by co-transfecting heavy chain and light chain expressing
543 plasmids using polyethylenimine transfection reagent and cultured for 5-7 days. Cells were
544 maintained in FreeStyle F17 expression medium supplemented at final concentrations of 0.1%

545 Pluronic Acid F-68 and 20% 4mM L-Glutamine. These cells were cultured at 37°C with 8% CO₂
546 saturation and shaking. After transfection and 5-7 days of culture, cell cultures were centrifuged
547 and supernatant was 0.45 µm filtered with Nalgene Rapid Flow Disposable Filter Units with PES
548 membrane. Filtered supernatant was run over a column containing Protein A agarose resin
549 equilibrated with PBS. The column was washed with PBS, and then antibodies were eluted with
550 100 mM Glycine HCl at 2.7 pH directly into a 1:10 volume of 1M Tris-HCl pH 8.0. Eluted
551 antibodies were buffer exchanged into PBS 3 times using Amicon Ultra centrifugal filter units
552 and concentrated. Antibodies were analyzed by SDS-PAGE. Additionally, antibodies 46472-1,
553 46472-2, 46472-3, 46472-4, 46472-6 and 46472-12 were assessed by size exclusion
554 chromatography on a Superdex 200 Increase 10/300 GL Sizing column with the AKTA FPLC
555 system.

556

557 **High-throughput Antibody Expression**

558 For high-throughput production of recombinant antibodies, approaches were used that are
559 designated as microscale. For antibody expression, microscale transfection were performed
560 (~1 ml per antibody) of CHO cell cultures using the Gibco ExpiCHO Expression System and a
561 protocol for deep 96-well blocks (Thermo Fisher Scientific). In brief, synthesized antibody-
562 encoding DNA (~2 µg per transfection) was added to OptiPro serum free medium (OptiPro
563 SFM), incubated with ExpiFectamine CHO Reagent and added to 800 µl of ExpiCHO cell
564 cultures into 96-deep-well blocks using a ViaFlo 384 liquid handler (Integra Biosciences). The
565 plates were incubated on an orbital shaker at 1,000 r.p.m. with an orbital diameter of 3 mm at
566 37 °C in 8% CO₂. The next day after transfection, ExpiFectamine CHO Enhancer and ExpiCHO
567 Feed reagents (Thermo Fisher Scientific) were added to the cells, followed by 4 d incubation for
568 a total of 5 d at 37 °C in 8% CO₂. Culture supernatants were collected after centrifuging the
569 blocks at 450g for 5 min and were stored at 4°C until use. For high-throughput microscale
570 antibody purification, fritted deep-well plates were used containing 25 µl of settled protein G

571 resin (GE Healthcare Life Sciences) per well. Clarified culture supernatants were incubated with
572 protein G resin for mAb capturing, washed with PBS using a 96-well plate manifold base
573 (Qiagen) connected to the vacuum and eluted into 96-well PCR plates using 86 μ l of 0.1 M
574 glycine-HCL buffer pH 2.7. After neutralization with 14 μ l of 1 M Tris-HCl pH 8.0, purified mAbs
575 were buffer-exchanged into PBS using Zeba Spin Desalting Plates (Thermo Fisher Scientific)
576 and stored at 4°C until use.

577

578 **ELISA**

579 To assess antibody binding, soluble protein was plated at 2 μ g/ml overnight at 4°C. The next
580 day, plates were washed three times with PBS supplemented with 0.05% Tween-20 (PBS-T)
581 and coated with 5% milk powder in PBS-T. Plates were incubated for one hour at room
582 temperature and then washed three times with PBS-T. Primary antibodies were diluted in 1%
583 milk in PBS-T, starting at 10 μ g/ml with a serial 1:5 dilution and then added to the plate. The
584 plates were incubated at room temperature for one hour and then washed three times in PBS-T.
585 The secondary antibody, goat anti-human IgG conjugated to peroxidase, was added at 1:10,000
586 dilution in 1% milk in PBS-T to the plates, which were incubated for one hour at room
587 temperature. Goat anti-mouse secondary was used for SARS-CoV specific control antibody
588 240CD (BEI Resources). Plates were washed three times with PBS-T and then developed by
589 adding TMB substrate to each well. The plates were incubated at room temperature for ten
590 minutes, and then 1N sulfuric acid was added to stop the reaction. Plates were read at 450 nm.
591 Data are represented as mean \pm SEM for one ELISA experiment. ELISAs were repeated 2 or
592 more times. The area under the curve (AUC) was calculated using GraphPad Prism 8.0.0. For
593 antibody 240CD, the following reagent was obtained through BEI Resources, NIAID, NIH:
594 Monoclonal Anti-SARS-CoV S Protein (Similar to 240C), NR-616.

595

596 **Competition ELISA**

597 Competition ELISAs were performed as described above, with some modifications. After coating
598 with antigen and blocking, 25 μ l of non-biotinylated competitor antibody was added to each well
599 at 10 μ g/ml and incubated at 37°C for 10 minutes. Then, without washing, 75 μ l biotinylated
600 antibody (final concentration of 1 μ g/ml) was added and incubated at 37°C for 1 hour. After
601 washing three times with PBS-T, streptavidin-HRP was added at 1:10,000 dilution in 1% milk in
602 PBS-T and incubated for 1 hour at room temperature. Plates were washed and substrate and
603 sulfuric acid were added as described above. ELISAs were repeated at least 2 times. Data is
604 shown as the % decrease in binding.

605

606 **Autoreactivity**

607 Monoclonal antibody reactivity to nine autoantigens (SSA/Ro, SS-B/La, Sm, ribonucleoprotein
608 (RNP), Scl 70, Jo-1, dsDNA, centromere B, and histone) was measured using the AtheNA Multi-
609 Lyte® ANA-II Plus test kit (Zeus scientific, Inc, #A21101). Antibodies were incubated with
610 AtheNA beads for 30min at concentrations of 50, 25, 12.5 and 6.25 μ g/mL. Beads were
611 washed, incubated with secondary and read on the Luminex platform as specified in the kit
612 protocol. Data were analyzed using AtheNA software. Positive (+) specimens received a score
613 >120, and negative (-) specimens received a score <100. Samples between 100-120 were
614 considered indeterminate.

615

616 **Mannose competition**

617 Mannose competition ELISAs were performed as described above with minor modifications.
618 After antigen coating and washing, nonspecific binding was blocked by incubation with 5% FBS
619 diluted in PBS for 1 hour at RT. Primary antibodies were diluted in 5% FBS-PBST +/- 1M D-(+)-
620 Mannose starting at 10 μ g/ml with a serial 1:5 dilution and then added to the plate for 1 hour at
621 RT. After washing, antibody binding was detected with goat anti-human IgG conjugated to
622 peroxidase and added at 1:10,000 dilution in 5% FBS in PBS-T to the plates. After 1 hour

623 incubation, plates were washed and substrate and sulfuric acid were added as described above.

624 Data shown is representative of three replicates.

625

626 **Epitope Mapping Visualization**

627 SARS-CoV-2 Spike (PDB-6VSB) was visualized using PyMOL software. Antibody epitopes
628 were visualized on the SARS-CoV-2 spike using a structure of the pre-fusion stabilized SARS-
629 CoV-2 S-2P construct⁵ modeled in the molecular graphics software PyMOL (The PyMOL
630 Molecular Graphics System, Version 2.3.5 Schrödinger, LLC).

631

632 **RTCA Neutralization Assay**

633 To assess for neutralizing activity against SARS-CoV-2 strain 2019 n-CoV/USA_WA1/2020
634 (obtained from the Centers for Disease Control and Prevention, a gift from N. Thornburg), we
635 used the high-throughput RTCA assay and xCelligence RTCA HT Analyzer (ACEA Biosciences)
636 that has been described previously¹¹. After obtaining a background reading of a 384-well E-
637 plate, 6,000 Vero-furin cells⁴⁸ were seeded per well. Sensograms were visualized using RTCA
638 HT software version 1.0.1 (ACEA Biosciences). One day later, equal volumes of virus were
639 added to antibody samples and incubated for 1 h at 37°C in 5% CO₂. mAbs were tested in
640 triplicate with a single (1:20) dilution. Virus–mAb mixtures were then added to Vero-furin cells in
641 384-well E-plates. Controls were included that had Vero-furin cells with virus only (no mAb) and
642 media only (no virus or mAb). E-plates were read every 8–12 h for 72 h to monitor virus
643 neutralization. At 32 h after virus-mAb mixtures were added to the E-plates, cell index values of
644 antibody samples were compared to those of virus only and media only to determine presence
645 of neutralization.

646

647 **Nano-luciferase Neutralization Assay**

648 A full-length SARS-CoV-2 virus based on the Seattle Washington isolate and a full-length
649 SARS-CoV virus based on the Urbani isolate were designed to express luciferase and was
650 recovered via reverse genetics and described previously^{49,50}. Viruses were titered in Vero E6
651 USAMRID cells to obtain a relative light units (RLU) signal of at least 10X the cell only control
652 background. Vero E6 USAMRID cells were plated at 20,000 cells per well the day prior in clear
653 bottom black walled 96-well plates (Corning 3904). Neutralizing antibody serum samples were
654 tested at a starting dilution of 1:40 and were serially diluted 4-fold up to eight dilution spots.
655 Antibody-virus complexes were incubated at 37C with 5% CO₂ for 1 hour. Following incubation,
656 growth media was removed and virus-antibody dilution complexes were added to the cells in
657 duplicate. Virus-only controls and cell-only controls were included in each neutralization assay
658 plate. Following infection, plates were incubated at 37C with 5% CO₂ for 48 hours. After the 48
659 hour incubation, cells were lysed and luciferase activity was measured via Nano-Glo Luciferase
660 Assay System (Promega) according to the manufacturer specifications. SARS-CoV and SARS-
661 CoV-2 neutralization titers were defined as the sample dilution at which a 50% reduction in RLU
662 was observed relative to the average of the virus control wells.

663

664 **SPR**

665 His-tagged SARS-CoV-2 RBD-SD1 was immobilized to a NiNTA sensorchip to a level of ~150
666 RUs using a Biacore X100. Serial dilutions of purified Fab 46472-12 were evaluated for binding,
667 ranging in concentration from 1 to 0.25 μ M. The resulting data were fit to a 1:1 binding model
668 using Biacore Evaluation Software.

669 **Fc Effector function Assays**

670 **Antibody-dependent Cellular Phagocytosis (ADCP)**

671 Antibody-dependent cellular phagocytosis (ADCP) was performed using biotinylated SARS-
672 CoV-2 or SARS-CoV S coated fluorescent neutravidin beads as previously described⁵¹. Briefly,

673 beads were incubated for two hours with antibodies at a starting concentration of 50µg/ml and
674 titrated five fold. CR3022 was used as a positive control while Palivizumab was used as a
675 negative control. Antibodies and beads were incubated with THP-1 cells overnight, fixed and
676 interrogated on the FACS Aria II. Phagocytosis score was calculated as the percentage of THP-
677 1 cells that engulfed fluorescent beads multiplied by the geometric mean fluorescence intensity
678 of the population in the FITC channel less the no antibody control.

679

680 **Antibody-dependent Cellular Trogocytosis (ADCT)**

681 ADCT was performed as described in and modified from a previously described study²⁹.
682 HEK293T cells transfected with a SARS-CoV-2 spike pcDNA vector were surface biotinylated
683 with EZ-Link Sulfo-NHS-LC-Biotin as recommended by the manufacturer. Fifty-thousand cells
684 per well were incubated with antibody for 30 minutes starting at 25µg/ml and titrated 5 fold.
685 CR3022 was used as a positive control with Palivizumab as a negative. Following a RPMI
686 media wash, these were then incubated with carboxyfluorescein succinimidyl ester (CFSE)
687 stained THP-1 cells (5 X10⁴ cells per well) for 1 hour and washed with 15mM EDTA/PBS
688 followed by PBS. Cells were then stained for biotin using Streptavidin-PE and read on a
689 FACS Aria II. Trogocytosis score was determined as the proportion of CFSE positive THP-1 cells
690 also positive for streptavidin-PE less the no antibody control.

691

692 **Antibody-dependent Complement Deposition (ADCD)**

693 Antibody-dependent complement deposition was performed as previously described⁵². Briefly
694 biotinylated SARS-Cov-2 S protein was coated 1:1 onto fluorescent neutravidin beads for 2
695 hours at 37 degrees. These beads were incubated with 100ug/ml of antibody for 1 hour and
696 incubated with guinea pig complement diluted 1 in 50 with gelatin/veronal buffer for 15 minutes
697 at 37 degrees. Beads were washed at 2000g twice in PBS and stained with anti-guinea pig C3b-
698 FITC, fixed and interrogated on a FACS Aria II. Complement deposition score was calculated as

699 the percentage of C3b-FITC positive beads multiplied by the geometric mean fluorescent
700 intensity of FITC in this population less the no antibody or heat inactivated controls.

701

702 **Antibody Prophylaxis - Murine Model of Infection**

703 For evaluating the prophylactic efficacy of mAbs, 12-month old female BALB/c mice
704 (BALB/cAnHsd; Envigo, stock number 047) were treated with 200 µg mAb intraperitoneally (i.p.)
705 12 hours prior to virus inoculation. The next day, mice were administered intranasally with 1×10^3
706 PFU or 1×10^4 PFU of SARS-CoV-2 MA10, respectively. Mice were monitored daily for weight
707 loss, morbidity, and mortality, and after four days, mice were sacrificed and lung tissue was
708 harvested for viral titer as measured by plaque assays. One lung lobe was taken for
709 pathological analysis and the other lobe was processed for qPCR and viral load determination
710 as previously described³¹. For viral plaque assays, the caudal lobe of the right lung was
711 homogenized in PBS, and the tissue homogenate was then serial-diluted onto confluent
712 monolayers of Vero E6 cells, followed by agarose overlay. Plaques were visualized with overlay
713 of Neutral Red dye on day 2 post infection. Gross pulmonary hemorrhage was observed at time
714 of tissue harvest and scored on a scale of 0 (no hemorrhage in any lobe, normal pink healthy
715 lung) to 4 (complete hemorrhage in all lobes of the lung, completely dark red lung).

716

717 For viral titer and hemorrhage score comparisons, an ordinary one-way ANOVA test with
718 multiple comparisons was performed using Prism software, GraphPad Prism version 8.0.

719

720 **ACE2 Binding Inhibition Assay**

721 Wells of 384-well microtiter plates were coated with purified recombinant SARS-CoV-2 S-2P
722 ectoprotein at 4°C overnight. Plates were blocked with 2% non-fat dry milk and 2% normal goat
723 serum in DPBS-T for 1 hr. Purified mAbs were diluted two-fold in blocking buffer starting from 10
724 µg/mL in triplicate, added to the wells (20 µL/well), and incubated at ambient temperature.

725 Recombinant human ACE2 with a C-terminal FLAG tag protein was added to wells at 2 µg/mL
726 in a 5 µL/well volume (final 0.4 µg/mL concentration of ACE2) without washing of antibody and
727 then incubated for 40 min at ambient temperature. Plates were washed, and bound ACE2 was
728 detected using HRP-conjugated anti-FLAG antibody and TMB substrate. ACE2 binding without
729 antibody served as a control. Experiment was done in biological replicate and technical
730 triplicates, shown is representative of one replicate with positive control mAb COV2-2196¹¹.

731

732 **Identification of Residue-level Mutants**

733 Potential cross-reactive epitopes were identified based on sequence and structural homology.
734 Reference sequences for each Coronavirus S were obtained either from NCBI for SARS-CoV-2
735 (YP_009724390.1) and MERS-CoV (YP_009047204.1) or from Uniprot for SARS-CoV (P59594)
736 of the spikes was then obtained using MUSCLE⁵³ and the amino acid similarity to SARS-CoV-2
737 at each residue position was calculated using the BLOSUM-62 scoring matrix⁵⁴. These scores
738 were then used to color each residue position on the SARS-CoV-2 S structure (PDB ID: 6VSB)
739 in PyMOL (Schrodinger, version 2.3.5) in order to visualize surface patches and linear epitopes
740 with structural homology. These conserved regions were then visualized on the other human
741 coronavirus spike structures by retrieving them from the Protein Databank (SARS-CoV: 5X5B,
742 MERS-CoV: 5W9I) and aligning them to the SARS-CoV-2 S structure. Finally, the residue N165
743 was part of a conserved surface patches and was mutated to alanine and tested for binding with
744 antibodies. The N709A mutant tested was previously described in Acharya et al., BioRxiv
745 (2020).

746

747 **QUANTIFICATION AND STATISTICAL ANALYSIS**

748 ELISA error bars (standard error of the mean) were calculated using GraphPad Prism version
749 8.0.0. ANOVA analysis (ordinary one way ANOVA with multiple comparisons) was performed on

750 viral load titers and hemorrhage scores from animal experiments using GraphPad Prism version

751 8.0.0. Details of the statistical analyses can be found in the main text and figure captions.

752

753

754

755

756

757

758

759

760

761

762

763

764 **KEY RESOURCES TABLE**

765

Journal Pre-proof

766
767
768
769
770
771
772
773
774
775
776
777
778
779
780
781

Journal Pre-proof

782 **REFERENCES**

- 783 1. Lu, R., Zhao, X., Li, J., Niu, P., Yang, B., Wu, H., Wang, W., Song, H., Huang, B., Zhu,
784 N., et al. (2020). Genomic characterisation and epidemiology of 2019 novel coronavirus:
785 implications for virus origins and receptor binding. *The Lancet* 395, 565–574.
- 786 2. Graham, R.L., and Baric, R.S. (2010). Recombination, Reservoirs, and the Modular
787 Spike: Mechanisms of Coronavirus Cross-Species Transmission. *JVI* 84, 3134–3146.
- 788 3. Bosch, B.J., van der Zee, R., de Haan, C.A.M., and Rottier, P.J.M. (2003). The
789 Coronavirus Spike Protein Is a Class I Virus Fusion Protein: Structural and Functional
790 Characterization of the Fusion Core Complex. *JVI* 77, 8801–8811.
- 791 4. Tortorici, M.A., and Velesler, D. (2019). Structural insights into coronavirus entry. In
792 *Advances in Virus Research*, (Elsevier), pp. 93–116.
- 793 5. Wrapp, D., Wang, N., Corbett, K.S., Goldsmith, J.A., Hsieh, C.-L., Abiona, O., Graham,
794 B.S., and McLellan, J.S. (2020). Cryo-EM structure of the 2019-nCoV spike in the
795 prefusion conformation. *Science* 367, 1260–1263.
- 796 6. Jiang, S., Hillyer, C., and Du, L. (2020). Neutralizing Antibodies against SARS-CoV-2
797 and Other Human Coronaviruses. *Trends in Immunology* 41, 355–359.
- 798 7. Krammer, F. (2020). SARS-CoV-2 vaccines in development. *Nature* 586, 516–527.
- 799 8. Li, F. (2016). Structure, Function, and Evolution of Coronavirus Spike Proteins. *Annu.*
800 *Rev. Virol.* 3, 237–261.
- 801 9. Brouwer, P.J.M., Caniels, T.G., van der Straten, K., Snitselaar, J.L., Aldon, Y., Bangaru,
802 S., Torres, J.L., Okba, N.M.A., Claireaux, M., Kerster, G., et al. (2020). Potent
803 neutralizing antibodies from COVID-19 patients define multiple targets of vulnerability.
804 *Science* 369, 643–650.
- 805 10. Chi, X., Yan, R., Zhang, J., Zhang, G., Zhang, Y., Hao, M., Zhang, Z., Fan, P., Dong, Y.,
806 Yang, Y., et al. (2020). A neutralizing human antibody binds to the N-terminal domain of
807 the Spike protein of SARS-CoV-2. *Science* 369, 650–655.

- 808 11. Zost, S.J., Gilchuk, P., Chen, R.E., Case, J.B., Reidy, J.X., Trivette, A., Nargi, R.S.,
809 Sutton, R.E., Suryadevara, N., Chen, E.C., et al. (2020). Rapid isolation and profiling of
810 a diverse panel of human monoclonal antibodies targeting the SARS-CoV-2 spike
811 protein. *Nat Med* 26, 1422–1427.
- 812 12. Pinto, D., Park, Y.-J., Beltramello, M., Walls, A.C., Tortorici, M.A., Bianchi, S., Jaconi, S.,
813 Culap, K., Zatta, F., De Marco, A., et al. (2020). Cross-neutralization of SARS-CoV-2 by
814 a human monoclonal SARS-CoV antibody. *Nature* 583, 290–295.
- 815 13. Rogers, T.F., Zhao, F., Huang, D., Beutler, N., Burns, A., He, W., Limbo, O., Smith, C.,
816 Song, G., Woehl, J., et al. (2020). Isolation of potent SARS-CoV-2 neutralizing
817 antibodies and protection from disease in a small animal model. *Science* 369, 956–963.
- 818 14. Chen, P., Nirula, A., Heller, B., Gottlieb, R.L., Boscia, J., Morris, J., Huhn, G., Cardona,
819 J., Mocherla, B., Stosor, V., et al. (2021). SARS-CoV-2 Neutralizing Antibody LY-
820 CoV555 in Outpatients with Covid-19. *N Engl J Med* 384, 229–237.
- 821 15. Cohen, M.S. (2021). Monoclonal Antibodies to Disrupt Progression of Early Covid-19
822 Infection. *N Engl J Med* 384, 289–291.
- 823 16. Weinreich, D.M., Sivapalasingam, S., Norton, T., Ali, S., Gao, H., Bhore, R., Musser,
824 B.J., Soo, Y., Rofail, D., Im, J., et al. (2021). REGN-COV2, a Neutralizing Antibody
825 Cocktail, in Outpatients with Covid-19. *N Engl J Med* 384, 238–251.
- 826 17. Liu, H., Wu, N.C., Yuan, M., Bangaru, S., Torres, J.L., Caniels, T.G., van Schooten, J.,
827 Zhu, X., Lee, C.-C.D., Brouwer, P.J.M., et al. (2020). Cross-Neutralization of a SARS-
828 CoV-2 Antibody to a Functionally Conserved Site Is Mediated by Avidity. *Immunity*
829 S1074761320304647.
- 830 18. Wec, A.Z., Wrapp, D., Herbert, A.S., Maurer, D.P., Haslwanter, D., Sakharkar, M.,
831 Jangra, R.K., Dieterle, M.E., Lilov, A., Huang, D., et al. (2020). Broad neutralization of
832 SARS-related viruses by human monoclonal antibodies. *Science* 369, 731–736.

- 833 19. Lv, H., Wu, N.C., Tsang, O.T.-Y., Yuan, M., Perera, R.A.P.M., Leung, W.S., So, R.T.Y.,
834 Chan, J.M.C., Yip, G.K., Chik, T.S.H., et al. (2020). Cross-reactive Antibody Response
835 between SARS-CoV-2 and SARS-CoV Infections. *Cell Reports* 31, 107725.
- 836 20. Zohar, T., and Alter, G. (2020). Dissecting antibody-mediated protection against SARS-
837 CoV-2. *Nat Rev Immunol* 20, 392–394.
- 838 21. Ng, K.W., Faulkner, N., Cornish, G.H., Rosa, A., Harvey, R., Hussain, S., Ulferts, R.,
839 Earl, C., Wrobel, A.G., Benton, D.J., et al. (2020). Preexisting and de novo humoral
840 immunity to SARS-CoV-2 in humans. *Science* 370, 1339–1343.
- 841 22. Yasui, F., Kohara, M., Kitabatake, M., Nishiwaki, T., Fujii, H., Tateno, C., Yoneda, M.,
842 Morita, K., Matsushima, K., Koyasu, S., et al. (2014). Phagocytic cells contribute to the
843 antibody-mediated elimination of pulmonary-infected SARS coronavirus. *Virology* 454–
844 455, 157–168.
- 845 23. Schäfer, A., Muecksch, F., Lorenzi, J.C.C., Leist, S.R., Cipolla, M., Bournazos, S.,
846 Schmidt, F., Maison, R.M., Gazumyan, A., Martinez, D.R., et al. (2021). Antibody
847 potency, effector function, and combinations in protection and therapy for SARS-CoV-2
848 infection in vivo. *Journal of Experimental Medicine* 218, e20201993.
- 849 24. Atyeo, C., Fischinger, S., Zohar, T., Slein, M.D., Burke, J., Loos, C., McCulloch, D.J.,
850 Newman, K.L., Wolf, C., Yu, J., et al. (2020). Distinct Early Serological Signatures Track
851 with SARS-CoV-2 Survival. *Immunity* 53, 524-532.
- 852 25. Loos, C., Atyeo, C., Fischinger, S., Burke, J., Slein, M.D., Streeck, H., Lauffenburger, D.,
853 Ryan, E.T., Charles, R.C., and Alter, G. (2020). Evolution of Early SARS-CoV-2 and
854 Cross-Coronavirus Immunity. *MSphere* 5, e00622-20.
- 855 26. Ou, X., Liu, Y., Lei, X., Li, P., Mi, D., Ren, L., Guo, L., Guo, R., Chen, T., Hu, J., et al.
856 (2020). Characterization of spike glycoprotein of SARS-CoV-2 on virus entry and its
857 immune cross-reactivity with SARS-CoV. *Nat Commun* 11, 1620.

- 858 27. Setliff, I., Shiakolas, A.R., Pilewski, K.A., Murji, A.A., Mapengo, R.E., Janowska, K.,
859 Richardson, S., Oosthuysen, C., Raju, N., Ronsard, L., et al. (2019). High-Throughput
860 Mapping of B Cell Receptor Sequences to Antigen Specificity. *Cell* 179, 1636-1646.
- 861 28. Yuan, M., Wu, N.C., Zhu, X., Lee, C.-C.D., So, R.T.Y., Lv, H., Mok, C.K.P., and Wilson,
862 I.A. (2020). A highly conserved cryptic epitope in the receptor binding domains of SARS-
863 CoV-2 and SARS-CoV. *Science* 368, 630–633.
- 864 29. Richardson, S.I., Crowther, C., Mkhize, N.N., and Morris, L. (2018). Measuring the ability
865 of HIV-specific antibodies to mediate trogocytosis. *Journal of Immunological Methods*
866 463, 71–83.
- 867 30. Dinnon, K.H., Leist, S.R., Schäfer, A., Edwards, C.E., Martinez, D.R., Montgomery,
868 S.A., West, A., Yount, B.L., Hou, Y.J., Adams, L.E., et al. (2020). A mouse-adapted
869 model of SARS-CoV-2 to test COVID-19 countermeasures. *Nature* 586, 560–566.
- 870 31. Leist, S.R., Dinnon, K.H., Schäfer, A., Tse, L.V., Okuda, K., Hou, Y.J., West, A.,
871 Edwards, C.E., Sanders, W., Fritch, E.J., et al. (2020). A Mouse-Adapted SARS-CoV-2
872 Induces Acute Lung Injury and Mortality in Standard Laboratory Mice. *Cell* 183, 1070-
873 1085.
- 874 32. Yu, J., Tostanoski, L.H., Peter, L., Mercado, N.B., McMahan, K., Mahrokhian, S.H.,
875 Nkolola, J.P., Liu, J., Li, Z., Chandrashekar, A., et al. (2020). DNA vaccine protection
876 against SARS-CoV-2 in rhesus macaques. *Science* 369, 806–811.
- 877 33. Zohar, T., and Alter, G. (2020). Dissecting antibody-mediated protection against SARS-
878 CoV-2. *Nat Rev Immunol* 20, 392–394.
- 879 34. Atyeo, C., Slein, M.D., Fischinger, S., Burke, J., Schäfer, A., Leist, S.R., Kuzmina, N.A.,
880 Mire, C., Honko, A., Johnson, R., et al. (2021). Dissecting strategies to tune the
881 therapeutic potential of SARS-CoV-2–specific monoclonal antibody CR3022. *JCI Insight*
882 6, e143129.

- 883 35. Bournazos, S., Klein, F., Pietzsch, J., Seaman, M.S., Nussenzweig, M.C., and Ravetch,
884 J.V. (2014). Broadly Neutralizing Anti-HIV-1 Antibodies Require Fc Effector Functions for
885 In Vivo Activity. *Cell* 158, 1243–1253.
- 886 36. Bournazos, S., DiLillo, D.J., Goff, A.J., Glass, P.J., and Ravetch, J.V. (2019). Differential
887 requirements for FcγR engagement by protective antibodies against Ebola virus. *Proc*
888 *Natl Acad Sci USA* 116, 20054–20062.
- 889 37. DiLillo, D.J., Palese, P., Wilson, P.C., and Ravetch, J.V. (2016). Broadly neutralizing
890 anti-influenza antibodies require Fc receptor engagement for in vivo protection. *Journal*
891 *of Clinical Investigation* 126, 605–610.
- 892 38. Lu, L.L., Suscovich, T.J., Fortune, S.M., and Alter, G. (2018). Beyond binding: antibody
893 effector functions in infectious diseases. *Nat Rev Immunol* 18, 46–61.
- 894 39. Winkler, E.S., Gilchuk, P., Yu, J., Bailey, A.L., Chen, R.E., Chong, Z., Zost, S.J., Jang,
895 H., Huang, Y., Allen, J.D., et al. (2021). Human neutralizing antibodies against SARS-
896 CoV-2 require intact Fc effector functions for optimal therapeutic protection. *Cell* 184,
897 1804-1820.e16.
- 898 40. Edwards, C.E., Yount, B.L., Graham, R.L., Leist, S.R., Hou, Y.J., Dinnon, K.H., Sims,
899 A.C., Swanstrom, J., Gully, K., Scobey, T.D., et al. (2020). Swine acute diarrhea
900 syndrome coronavirus replication in primary human cells reveals potential susceptibility
901 to infection. *Proc Natl Acad Sci U S A* 117, 26915–26925.
- 902 41. Menachery, V.D., Yount, B.L., Sims, A.C., Debbink, K., Agnihothram, S.S., Gralinski,
903 L.E., Graham, R.L., Scobey, T., Plante, J.A., Royal, S.R., et al. (2016). SARS-like WIV1-
904 CoV poised for human emergence. *Proc Natl Acad Sci USA* 113, 3048–3053.
- 905 42. Menachery, V.D., Yount, B.L., Debbink, K., Agnihothram, S., Gralinski, L.E., Plante, J.A.,
906 Graham, R.L., Scobey, T., Ge, X.-Y., Donaldson, E.F., et al. (2015). A SARS-like cluster
907 of circulating bat coronaviruses shows potential for human emergence. *Nat Med* 21,
908 1508–1513.

- 909 43. Song, Z., Xu, Y., Bao, L., Zhang, L., Yu, P., Qu, Y., Zhu, H., Zhao, W., Han, Y., and Qin,
910 C. (2019). From SARS to MERS, Thrusting Coronaviruses into the Spotlight. *Viruses* 11,
911 59.
- 912 44. Zohar, T., Loos, C., Fischinger, S., Atyeo, C., Wang, C., Slein, M.D., Burke, J., Yu, J.,
913 Feldman, J., Hauser, B.M., et al. (2020). Compromised Humoral Functional Evolution
914 Tracks with SARS-CoV-2 Mortality. *Cell* 183, 1508-1519.e12.
- 915 45. Pallesen, J., Wang, N., Corbett, K.S., Wrapp, D., Kirchdoerfer, R.N., Turner, H.L.,
916 Cottrell, C.A., Becker, M.M., Wang, L., Shi, W., et al. (2017). Immunogenicity and
917 structures of a rationally designed prefusion MERS-CoV spike antigen. *Proc Natl Acad*
918 *Sci USA* 114, E7348–E7357.
- 919 46. Alamyar, E., Duroux, P., Lefranc, M.-P., and Giudicelli, V. (2012). IMGT® Tools for the
920 Nucleotide Analysis of Immunoglobulin (IG) and T Cell Receptor (TR) V-(D)-J
921 Repertoires, Polymorphisms, and IG Mutations: IMGT/V-QUEST and IMGT/HighV-
922 QUEST for NGS. *Methods Mol Biol.* 882, 569-604.
- 923 47. Gupta, N.T., Vander Heiden, J.A., Uduman, M., Gadala-Maria, D., Yaari, G., and
924 Kleinstein, S.H. (2015). Change-O: a toolkit for analyzing large-scale B cell
925 immunoglobulin repertoire sequencing data. *Bioinformatics* 31, 3356–3358.
- 926 48. Mukherjee, S., Sirohi, D., Dowd, K.A., Chen, Z., Diamond, M.S., Kuhn, R.J., and
927 Pierson, T.C. (2016). Enhancing dengue virus maturation using a stable furin over-
928 expressing cell line. *Virology* 497, 33–40.
- 929 49. Scobey, T., Yount, B.L., Sims, A.C., Donaldson, E.F., Agnihothram, S.S., Menachery,
930 V.D., Graham, R.L., Swanstrom, J., Bove, P.F., Kim, J.D., et al. (2013). Reverse
931 genetics with a full-length infectious cDNA of the Middle East respiratory syndrome
932 coronavirus. *Proc Natl Acad Sci* 110, 16157–16162.
- 933 50. Yount, B., Curtis, K.M., Fritz, E.A., Hensley, L.E., Jahrling, P.B., Prentice, E., Denison,
934 M.R., Geisbert, T.W., and Baric, R.S. (2003). Reverse genetics with a full-length

- 935 infectious cDNA of severe acute respiratory syndrome coronavirus. *Proc Natl Acad Sci*
936 100, 12995–13000.
- 937 51. Ackerman, M.E., Moldt, B., Wyatt, R.T., Dugast, A.-S., McAndrew, E., Tsoukas, S., Jost,
938 S., Berger, C.T., Sciaranghella, G., Liu, Q., et al. (2011). A robust, high-throughput
939 assay to determine the phagocytic activity of clinical antibody samples. *Journal of*
940 *Immunological Methods* 366, 8–19.
- 941 52. Fischinger, S., Fallon, J.K., Michell, A.R., Broge, T., Suscovich, T.J., Streeck, H., and
942 Alter, G. (2019). A high-throughput, bead-based, antigen-specific assay to assess the
943 ability of antibodies to induce complement activation. *Journal of Immunological Methods*
944 473, 112630.
- 945 53. Madeira, F., Park, Y. mi, Lee, J., Buso, N., Gur, T., Madhusoodanan, N., Basutkar, P.,
946 Tivey, A.R.N., Potter, S.C., Finn, R.D., et al. (2019). The EMBL-EBI search and
947 sequence analysis tools APIs in 2019. *Nucleic Acids Research* 47, W636–W641.
- 948 54. Henikoff, S., and Henikoff, J.G. (1992). Amino acid substitution matrices from protein
949 blocks. *Proc Natl Acad Sci* 89, 10915–10919.
- 950 55. Baca, M., Presta, L.G., O'Connor, S.J., and Wells, J.A. (1997). Antibody Humanization
951 Using Monovalent Phage Display. *Journal of Biological Chemistry* 272, 10678–10684.
- 952 56. Walls, A.C., Xiong, X., Park, Y.-J., Tortorici, M.A., Snijder, J., Quispe, J., Cameroni, E.,
953 Gopal, R., Dai, M., Lanzavecchia, A., et al. (2019). Unexpected Receptor Functional
954 Mimicry Elucidates Activation of Coronavirus Fusion. *Cell* 176, 1026-1039.e15.
- 955 57. Tang, X.-C., Agnihothram, S.S., Jiao, Y., Stanhope, J., Graham, R.L., Peterson, E.C.,
956 Avnir, Y., Tallarico, A.S.C., Sheehan, J., Zhu, Q., et al. (2014). Identification of human
957 neutralizing antibodies against MERS-CoV and their role in virus adaptive evolution.
958 *Proceedings of the National Academy of Sciences* 111, E2018–E2026.

Highlights and eTOC blurb

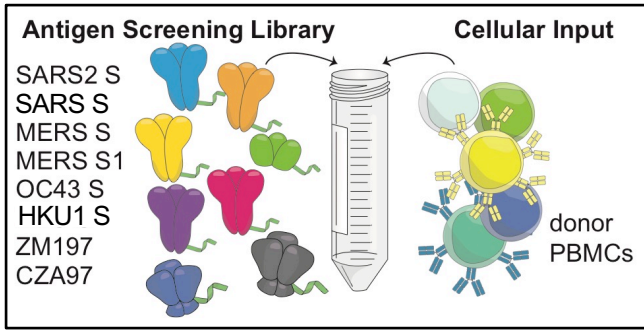
Highlights

- Applied LIBRA-seq to PBMCs from a recovered SARS-CoV donor
- Identified six cross-reactive CoV mAbs that target distinct domains on SARS-CoV-2 spike
- Characterized mAbs with effector functions in SARS-CoV-2 murine infection model

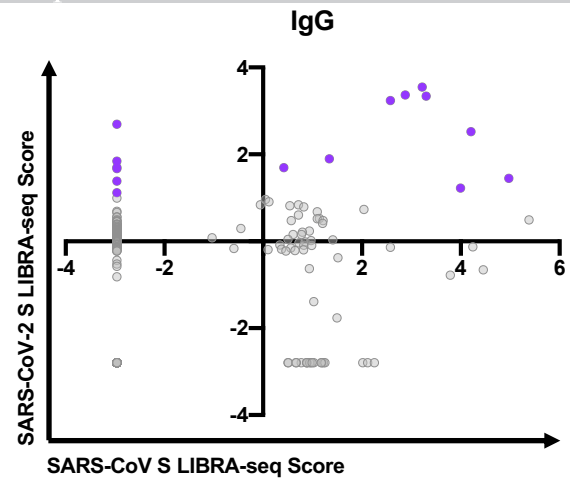
eTOC blurb

Shiakolas et al. demonstrate that cross-reactive coronavirus antibodies induced by natural infection display a spectrum of epitope specificities across the spike protein and exhibit *in vitro* and *in vivo* anti-viral functions.

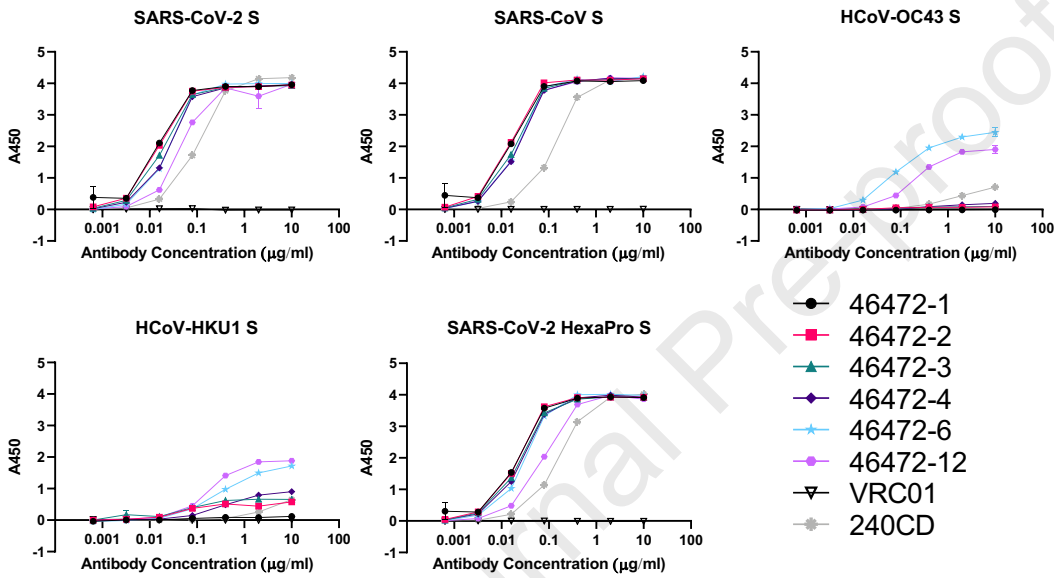
A



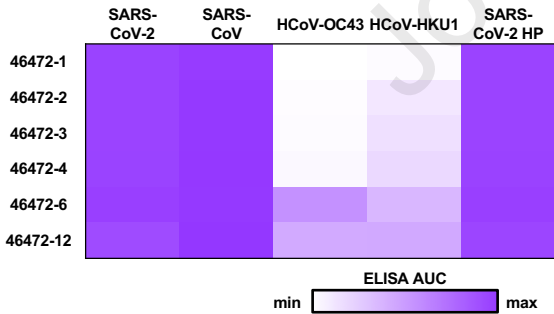
D

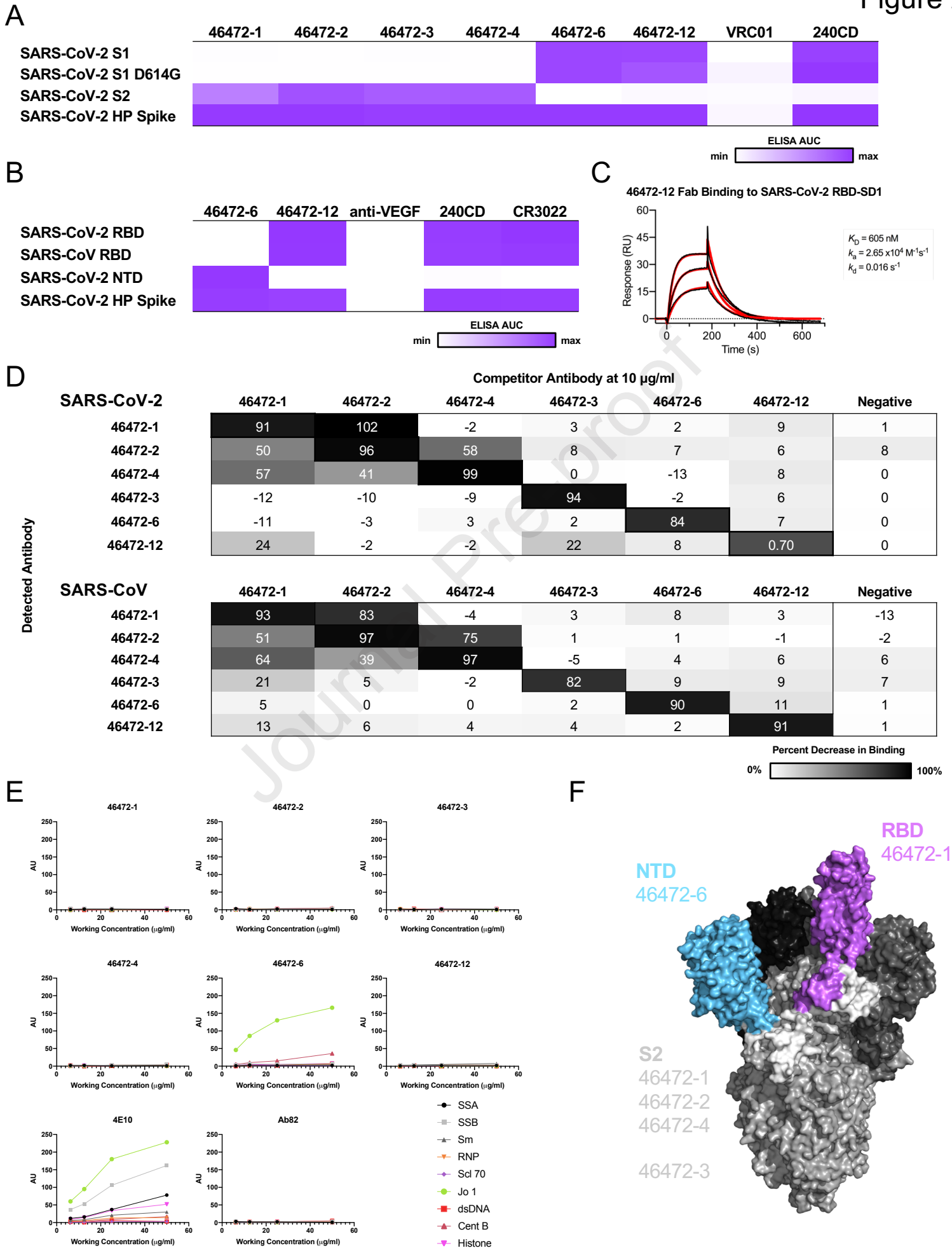


C

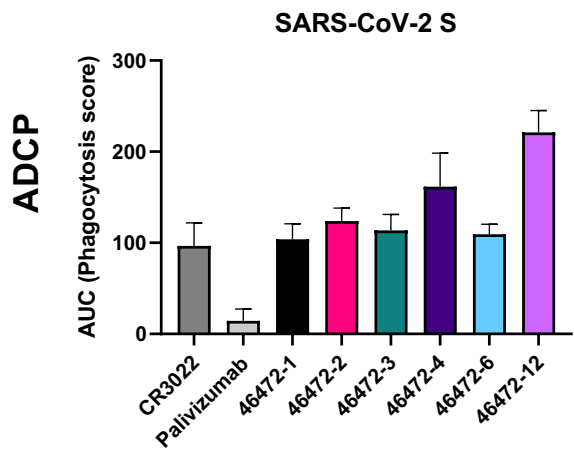


D

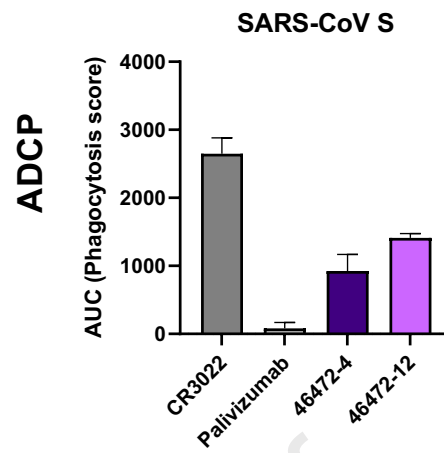




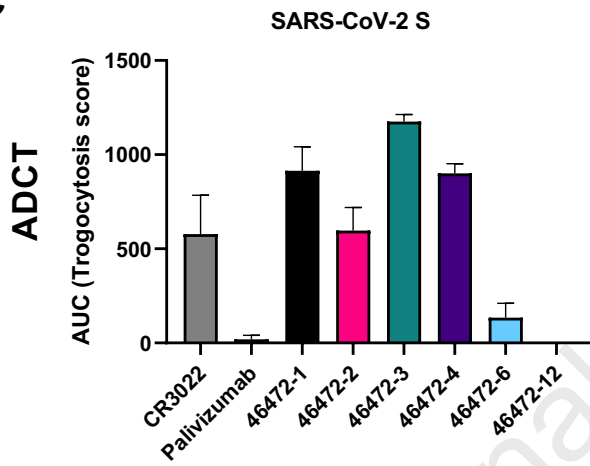
A



B



C



D

